JOURNAL OF GEOPHYSICAL RESEARCH, VOL. 106, NO. C4, PAGES 6895–6916, APRIL 15, 2001

Influence of precipitation minus evaporation and Bay of Bengal rivers on dynamics, thermodynamics, and mixed layer physics in the upper Indian Ocean

Weiqing Han
Program in Atmospheric and Oceanic Sciences, University of Colorado, Boulder, Colorado

Julian P. McCreary Jr.
International Pacific Research Center, University of Hawaii, Honolulu, Hawaii

Kevin E. Kohler
Oceanographic Center, Nova Southeastern University, Dania, Florida

Abstract. A $4^1/_2$-layer model with active thermodynamics and mixed layer physics is used to examine how salinity distributions forced by precipitation $\mathcal{P}$ minus evaporation $\mathcal{E}$ and by river runoff in the Bay of Bengal affect dynamics, thermodynamics, and mixed layer physics in the upper Indian Ocean. Each of the four active layers represents a distinct water mass type: the surface mixed layer, the seasonal thermocline (barrier layer in the tropics), the thermocline, and upper intermediate water. Waters are allowed to transfer between layers by interfacial velocities w_1, w_2, and w_3. Velocity w_1 parameterizes entrainment and detrainment from the surface mixed layer, and it is determined largely by *Kraus and Turner* [1967] physics. Velocity w_2 is primarily a parameterization of subduction. In regions where precipitation is strong enough for $\mathcal{P} - \mathcal{E} > 0$, forcing by $\mathcal{P} - \mathcal{E}$ thins the surface mixed layer (layer 1) because of decreased entrainment, and thus thickens the seasonal thermocline (layer 2, a barrier layer). Additionally, surface currents generally strengthen, T_2 warms considerably, and sea surface temperature (SST) increases somewhat, resulting in temperature inversions at some locations in the southern bay and eastern equatorial ocean. This forcing also causes large temperature changes in the thermocline (layer 3), primarily because of heating or cooling by anomalous subduction. During the Southwest Monsoon, forcing by inflow from Bay of Bengal rivers increases SST by 0.5°–1°C along the northeast coast of India. This is because coastal Kelvin waves driven by the Ganges-Brahmaputra River inflow suppress coastal upwelling there. During the Northeast Monsoon, fresh river water is carried southward by the East India Coastal Current (EICC), raising sea level along the coast and strengthening the EICC by 10 $\mathrm{cm\,s^{-1}}$. The river water decreases entrainment around the perimeter of the bay during winter, thereby thinning the surface mixed layer, increasing T_2, and resulting in temperature inversions in the northwestern bay. River inflow also causes significant temperature anomalies in layer 3 by affecting subduction.

1. Introduction

Salinity variations influence the stratification of the ocean and therefore its mixed layer physics, dynamics, and thermodynamics. Three major processes determine salinity distributions in the upper Indian Ocean: precipitation $\mathcal{P}$ and evaporation $\mathcal{E}$, river runoff in the Bay of Bengal, and fresher waters from the Indonesian Throughflow. Effects due to the throughflow have been investigated in several previous studies [*Godfrey and Golding*, 1981; *Kundu and McCreary*, 1986; *Hirst and Godfrey*, 1993; *McCreary et al.*, 1993, hereinafter referred to as MKM; *Murtugudde et al.*, 1998; *Schiller et al.*, 1998; *Han and McCreary*, 2001]. Here then we focus on discussing effects forced by $\mathcal{P} - \mathcal{E}$ and river runoff.

To date, there are few modeling studies that investigate effects due to $\mathcal{P} - \mathcal{E}$ in the Indian Ocean. A

Paper number 2000JC000403.
0148-0227/01/2000JC000403$09.00

number of studies include $\mathcal{P} - \mathcal{E}$ as part of the model forcing [*Anderson et al.*, 1991; *Godfrey and Weaver*, 1991; *Semtner and Chervin*, 1992; *Anderson and Carrington*, 1993; *Vinayachandran*, 1995; *Vinayachandran et al.*, 1999], but the specific effects that result from $\mathcal{P} - \mathcal{E}$ are not explicitly examined in any of them. *Murtugudde and Busalacchi* [1998] discuss how precipitation and the resulting salinity distributions affect sea surface temperature (SST) and mixed layer processes in the tropical Atlantic, Pacific, and Indo-Pacific regions. *Han et al.* [1999] (hereinafter referred to as HMAM) noted the strong influence that precipitation has on the eastward flowing equatorial surface current in the Indian Ocean during the fall (the fall Wyrtki Jet). In the Pacific Ocean, *Vialard and Delecluse* [1998] studied barrier layer formation and variability, and *Yang et al.* [1999] tested the sensitivity of the tropical Pacific Ocean to precipitation-induced freshwater flux.

Shetye et al. [1996] suggested that the thin surface mixed layer present in the northern bay throughout the year results from freshwater influx by rivers. This layer cools rapidly in winter, resulting in near-surface temperature inversions at about two thirds of the stations taken during December. They also hypothesized that runoff from the Ganges-Brahmaputra river system significantly strengthens the West India Coastal Current (WICC) during the Northeast Monsoon by causing an across-shelf salinity gradient along the coast. *McCreary et al.* [1997] theoretically investigated coastal circulations driven by river outflow in general. Modeling studies that specifically investigate the influences of the Ganges-Brahmaputra and any other Bay of Bengal rivers have not yet been carried out.

In this study we use an ocean model to investigate how salinity variations caused by $\mathcal{P} - \mathcal{E}$ and rivers affect the upper Indian Ocean. The model is a nonlinear, $4\frac{1}{2}$-layer, reduced gravity system. It is essentially a general circulation model (GCM) of intermediate complexity, differing from the most sophisticated GCMs in use today in that it has a limited vertical resolution (only 4 degrees of freedom). The model's simplicity is an advantage in that it is computationally efficient and hence easier to isolate basic processes. At the same time the model is sophisticated enough to develop solutions that compare well with observations, often remarkably so. In a companion paper, *Han and McCreary* [2001] describe effects of five different salinity forcings, including $\mathcal{P} - \mathcal{E}$ and the Bay of Bengal rivers. It is helpful, but not essential, to read this paper first.

The rest of the paper is organized as follows. Section 2 provides a detailed description of the $4\frac{1}{2}$-layer model. Section 3 describes a solution without any salinity forcing, pointing out deficiencies due to this lack. Section 4 examines effects due to $\mathcal{P} - \mathcal{E}$ forcing, and section 5 assesses influences caused by the Bay of Bengal rivers. Finally, section 6 provides a summary and conclusions.

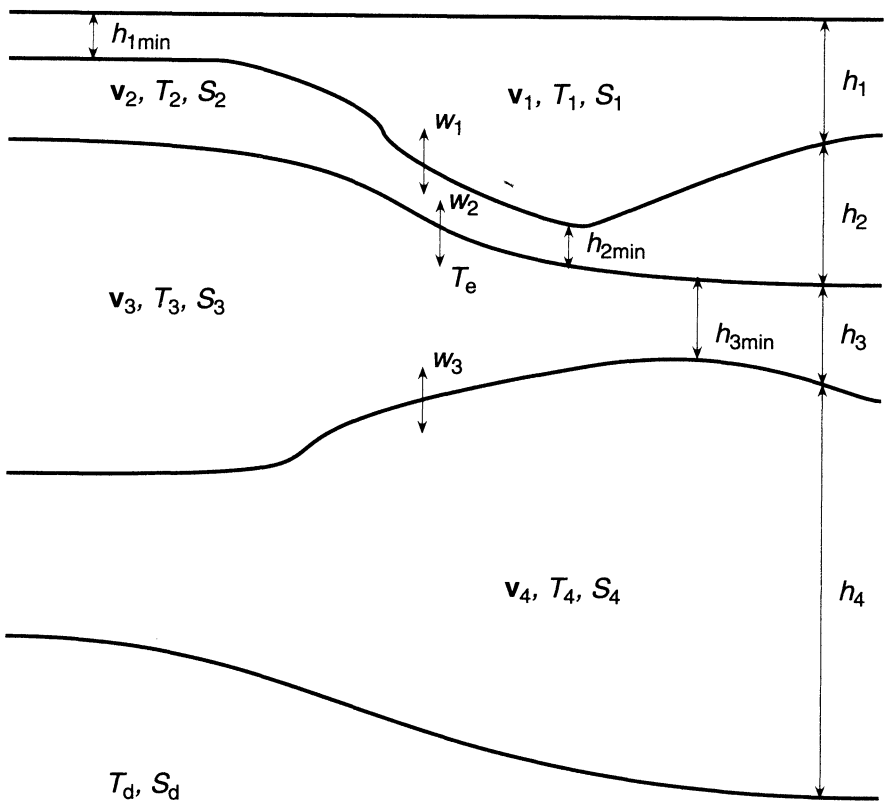

Figure 1. A schematic diagram illustrating the layer structure of the $4\frac{1}{2}$-layer model.

2. Model Ocean

The model is discussed in detail by *Han* [1999] and *Han et al.* [1999]. Here we discuss only those aspects necessary for understanding how salinity affects ocean processes.

2.1. Structure

Figure 1 illustrates the model's structure. It consists of four active layers with thicknesses h_i (i = 1–4 is a layer index), temperatures T_i, salinities S_i, and velocities $\mathbf{v}_i = (u_i, v_i)$, overlying a deep, quiescent ocean with temperature T_d and salinity S_d where pressure gradients are assumed to vanish (the "half" layer). The density of layer i and of the deep ocean (with subscript i replaced by d) is

$$\rho_i = \rho_0(1 + \alpha_t T_i + \alpha_s S_i), \tag{1}$$

where $\rho_0 = 1$ gm cm^{-3}, $\alpha_t = -2.5 \times 10^{-4}$ °C^{-1}, and $\alpha_s = 8 \times 10^{-4}$ psu^{-1}. The w_i fields are velocities at the bases of layers 1–3 that specify how water transfers across the interfaces between the layers. They contain terms that represent physical processes, w_k, w_s (both defined below) and w_r. Velocity w_r models mixing caused by strong shear between the upper layers; it acts to increase h_1 until it is thick enough for the bulk Richardson number of layer 1 to be greater than or equal to 0.4. In addition, the w_i fields also contain "correction" velocities w_{ic} that prevent layers from becoming thinner than prescribed minimum values, $h_{1\min} = h_{2\min} = 10$ m and $h_{3\min} = 50$ m. Typically, w_{1c} is active in upwelling regions where dynamical processes drive a divergent flow, and w_{2c} is active where entrainment thickens layer 1 significantly.

The T_i and S_i fields are allowed to vary in response to both surface fluxes and across-layer transfer by the w_i fields, so that the layers are not isopycnal ones. It is more appropriate rather, to interpret them as corresponding to distinct oceanic regions or water mass types, namely, the surface mixed layer, seasonal thermocline or barrier layer, thermocline, and upper intermediate water in layers 1–4, respectively. Outside the tropics the region between the mixed layer and the thermocline is known as the seasonal thermocline (layer 2) because it develops in the spring when the mixed layer thins. In the tropics it is referred to as the "barrier" layer because it blocks direct exchange between the mixed layer and the thermocline [*Lukas and Lindstrom*, 1991].

2.2. Processes

2.2.1. Across-interface velocities. Salinity forcings strongly affect the model through their influence on $w_1 = w_k + w_{1c} + w_r$, largely by altering w_k. Velocity w_k is determined by *Kraus and Turner* [1967] physics according to

$$w_k = \begin{cases} \dfrac{P}{\frac{1}{2}gh_1\Delta\rho'}, & P > 0, \\ \dfrac{h_{mo} - h_1^-}{2\Delta t}, & P \le 0, \end{cases} \tag{2a}$$

where

$$P = \rho_0 m u_*^3 - \tfrac{1}{2}gh_1\rho_0\left[-\alpha_t\frac{Q_1}{\rho_0 C_p} + \alpha_s(P-E)S_1\right] \tag{2b}$$

is the production of turbulent kinetic energy, h_{mo} is the Monin-Obukhov depth obtained by solving (2b) for h_1 when $P = 0$, $g = 980$ cm s^{-2} is the acceleration of gravity, and $\Delta\rho'$ is the density jump at the base of the mixed layer. In equations (2a) and (2b) h_1^- is the layer 1 thickness at the previous time level, $\Delta t = 0.8$ hours is the model time step, u_* is the oceanic friction velocity, $m = 1$ is the wind-stirring coefficient, and $C_p = 1$ cal gm^{-1} °C^{-1} is the specific heat of water. According to (2a), layer 1 entrains water from layer 2 when $P > 0$ and detrains instantly (i.e., in one time step of the integration) to the Monin-Obukhov depth h_{mo} when $P \le 0$. Salinity influences w_k by altering $\Delta\rho'$ and through the $\mathcal{P}-\mathcal{E}$ term in P.

Velocity w_2 has two forms. It is given by $w_k + w_{2c}$ when $h_2 = h_{2\min}$, a situation when layer 2 essentially vanishes or, equivalently, becomes part of layer 3. It is equal to w_s when $h_2 > h_{2\min}$ and the layer exists. In this case, w_s parameterizes the rate at which layer 2 water subducts into the thermocline layer. It is

$$w_s = -\frac{Q_1\theta(Q_1)}{Q_0}\frac{(h_1+h_2-h_d)^2}{t_d h_d} \times \theta(h_1+h_2-h_d)\,\theta(|y|-5^\circ), \tag{3}$$

where $t_d = 180$ days is the subduction time scale, $h_d = 65$ m is the subduction reference depth, $Q_0 = 40$ W m^{-2} is a scaling parameter, and θ is a step function. Salinity influences w_s indirectly by changing $h_1 + h_2$, as will be discussed next.

2.2.2. Layer thicknesses and temperatures. Equations for layer thickness and temperature are

$$h_{it} + \boldsymbol{\nabla}\cdot(h_i\mathbf{v}_i) - \kappa_h\nabla^2 h_i + \kappa_4\nabla^4 h_i = w_i - w_{i-1} + \delta_{i1}(\mathcal{P}-\mathcal{E}), \tag{4a}$$

and

$$\begin{aligned} T_{it} + \mathbf{v}_i\cdot\boldsymbol{\nabla}T_i - \kappa_t\nabla^2 T_i + \kappa_4\nabla^4 h_i &= \frac{Q_i}{\rho_0 C_p h_i} \\ &+ \frac{w_i^+}{h_i}(T_{i+1}-T_i) - \frac{w_{i-1}^-}{h_i}(T_{i-1}-T_i) \\ &+ \delta_{i3}\frac{\gamma_t}{h_3}(T_4-T_3) + \delta_{i4}\frac{\gamma_t}{h_4}(T_3-2T_4+T_d) \\ &+ \delta_{i2}\frac{w_2^+}{h_2}(T_e-T_3) - \delta_{i3}\frac{w_2^+}{h_3}(T_e-T_3), \end{aligned} \tag{4b}$$

where $\kappa_h = 10^7$ cm^2 s^{-1}, $\kappa_t = 5 \times 10^7$ cm^2 s^{-1}, and $\kappa_{h4} = \kappa_{t4} = 10^{21}$ cm^4 s^{-1} are Laplacian and biharmonic mixing coefficients, $w_i^+ = \max(w_i, 0)$ and $w_i^- = \min(w_i, 0)$ are the positive and negative parts of w_i, $\gamma_t = 3.3 \times 10^{-4}$ m day^{-1} is a diffusion coefficient, Q_i is the heating in layer i, δ_{ij} is a Kronecker delta symbol (δ_{ij} is 1 if $i = j$ and is 0 otherwise), and $w_0 = w_4 = 0$.

Temperature T_e is the temperature of the water that is entrained from layer 3 into layer 2. Because it is taken from the top of the thermocline layer, it is typically warmer than the average temperature of the thermocline, T_3, itself. It is defined by

$$T_e = \max\left[\mathrm{SST}_{\min}(y) - 3^\circ\mathrm{C},\ T_3\right], \tag{5}$$

where $\mathrm{SST}_{\min}(y)$ is the minimum value of observed SST along any latitude line y (see MKM, p. 187). A consequence of this specification is that layer 3 is cooled when its water is entrained into layer 2 since water warmer than T_3 is removed from the layer, and the last term in (4b) describes this cooling process. Specifying $T_e \geq T_3$ in this way is necessary to ensure that SST does not become too cold in strong upwelling regions (such as off Somalia).

According to (4a), changes of layer thickness are caused by convergence and divergence of mass, horizontal mixing, entrainment, and detrainment. The h_1 field is also affected by mass gain or loss through the ocean surface due to $\mathcal{P}-\mathcal{E}$, but that amount is negligible. Temperature variations (equation (4b)) are forced by heat fluxes (Q_i term) and affected by horizontal advection and mixing, entrainment from the underlying layer (w_i^+ terms), detrainment (subduction) from the overlying layer (w_{i-1}^+ terms), and vertical mixing between layers (γ_t terms). In both (4a) and (4b), horizontal mixing and diffusion terms are small in comparison to the other terms.

2.2.3. Currents and sea level. Salinity variations influence surface currents by changing h_1 and the depth-averaged pressure gradient force in layer 1, namely,

$$\frac{\langle \nabla p_1 \rangle}{\rho_0} = g\left(\nabla d + \frac{h_1}{2\rho_0}\nabla\rho_1\right), \tag{6}$$

where

$$d = \frac{1}{\rho_0}\sum_{i=1}^{4}(\rho_d - \rho_i)h_i \tag{7}$$

is the model sea level. Specifically, salinity forcing can enhance (weaken) the surface Ekman drift

$$u_{ek} = \frac{\tau^y}{f\rho_0 h_1}, \qquad v_{ek} = -\frac{\tau^x}{f\rho_0 h_1}, \tag{8}$$

by decreasing (increasing) h_1, and it can alter the geostrophic current,

$$u_g = -\frac{p_{1y}}{\rho_0 f}, \qquad v_g = \frac{p_{1x}}{\rho_0 f}, \tag{9}$$

through its influence on $\langle \nabla p_1 \rangle$.

2.3. Forcing and Numerics

The wind stress $\tau = \rho_a C_D|\mathbf{V}|\mathbf{V}$ used to force the model is the Florida State University (FSU) monthly mean pseudostress $|\mathbf{V}|\mathbf{V}$ averaged from 1970 to 1996 [*Legler et al.*, 1989], with $\rho_a = 0.001175\ \mathrm{gm\,cm^{-3}}$ and $C_D = 0.0015$. Precipitation $\mathcal{P}$ is provided by *Legates and Willmott* [1990; see *Han and McCreary*, 2001, Figure 2]. The thermal forcing is calculated from climatological fields of incoming short-wave radiation Q_{sw}, outgoing long-wave radiation Q_{lw}, air temperature T_a, specific humidity q_a, and scalar wind w_{sc} prepared by *Rao et al.* [1989, 1991]. Sensible and latent heat fluxes (Q_{sen} and Q_e) are then determined from these fields using standard bulk formulae and model SST, T_1 [*McCreary and Kundu*, 1989; MKM]. The incoming radiation Q_{sw} is represented as the sum of penetrating and nonpenetrating parts, with the former given by $\phi Q_{sw}e^{kz}$, where $\phi = 0.237$ and $k = 0.067\ \mathrm{m}^{-1}$. Heating Q_i of subsurface layers results from this process.

The model basin resembles the actual Indian Ocean north of 29°S, and it is shown in most of the panels that display the solution. Boundary conditions are described in detail by *Han and McCreary* [2001] and *Han et al.* [1999]. Solutions are obtained on a grid of dimension $\Delta x = \Delta y = 55$ km and are integrated forward in time for a period of 60 years, by which time solutions approach equilibrium. Figures 2–13 and plates 1–4 shown in later sections are from year 60 of their integrations.

3. Solution Without Salinity Forcing

In this section we discuss a solution without any external forcing of salinity. It serves as a reference point for understanding the influences of salinity forcing discussed in later sections, and we refer to it as the background run (solution BR). It is obtained by setting $\mathcal{P}-\mathcal{E} = 0$ in (2b) and in the equation for S_1 [see *Han and McCreary*, 2001]. Here we compare solution BR with observations, focusing on its deficiencies, particularly those that are diminished when salinity forcings are added. The upper layer circulations in solution BR are, in fact, very similar to those in the MKM solution, which also lacked salinity forcing. Interested readers can consult MKM for additional details.

3.1. Thicknesses

Figure 2 (left) shows mixed layer thickness from solution BR (h_1) and Figure 2 (right) shows mixed layer thickness calculated from the *Levitus and Boyer* [1994] and *Levitus et al.* [1994] data set (h_m) during January, April, July, and October. Thickness h_m is defined to be the first depth where density is $2.5\times10^{-4}\ \mathrm{gm\,cm^{-3}}$ greater than the surface density, an amount equivalent to the density change caused by a temperature decrease of 1°C.

In the Arabian Sea, h_1 varies semiannually, thickening to more than 100 m during the peaks of the Northeast and Southwest Monsoons and thinning to 10–40 m during spring and fall, consistent with h_m. In the Bay of Bengal, however, h_1 is much thicker than h_m during the winter, being > 100 m in the western bay during Jan-

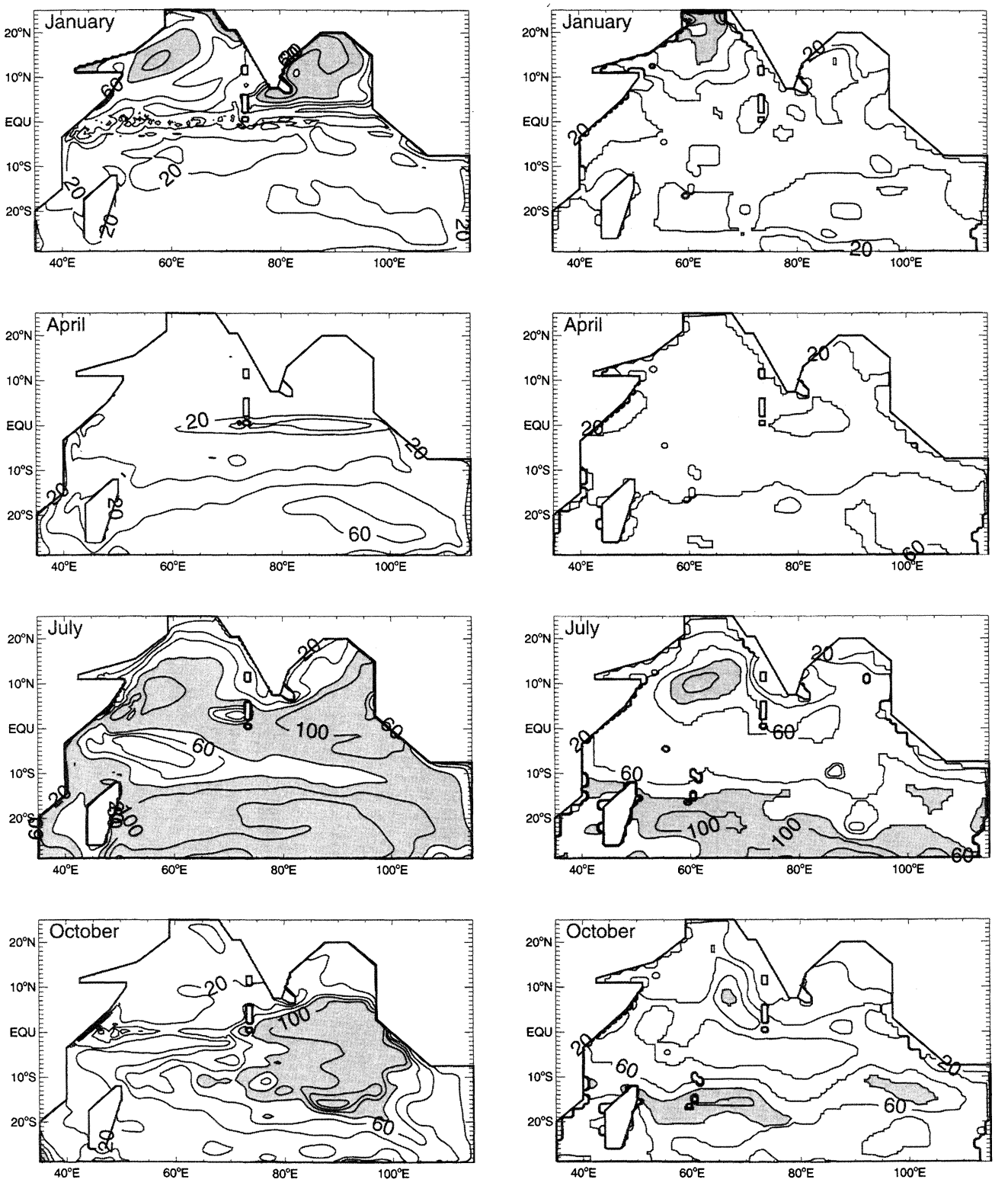

Figure 2. (left) Thickness h_1 from solution BR and (right) mixed layer thickness h_m calculated from *Levitus and Boyer* [1994] and *Levitus et al.* [1994] data for January, April, July, and October. The contour interval is 20 m. Values > 80 m are shaded.

uary when h_m is only 10–20 m. Similarly, in the central and eastern equatorial ocean, h_1 is much thicker than h_m during late spring, summer, and fall. In the latter case, h_1 thickens because equatorial westerlies during spring and fall cause convergence at the equator and push the thermocline downward. This signal propagates via Kelvin waves along the eastern boundary into the Bay of Bengal [see *McCreary et al.*, 1996; MKM]. South of 10°S, the annual cycle of h_1 compares reasonably well with the observations, except that it tends to be somewhat too thick during the austral winter. Note that h_1 is noisy along the equator during January when it is thin and u_1 is westward and strong (Figure 4). The reason for this noise is entrainment due to w_r at locations where current shear between the first two layers is sufficiently strong. (The Δh_1 and Δh_2 fields in Plates 1 and 3 below are also noisy along the equator during January for a similar reason.)

Typically, the h_2 field mirrors the h_1 field. In particular, at locations where h_1 is thick, h_2 is thin and often attains its minimum value $h_{2\,\min}$. Thus in solution BR there is little or no barrier layer in the eastern tropical ocean, a property that contrasts with the observations (P. Webster et al., The Joint Air-Sea Monsoon Interaction Experiment (JASMINE), 2, Results from the field phase, manuscript in preparation, 2001, hereinafter referred to as P. Webster et al., manuscript in preparation, 2001).

3.2. Temperatures

Figure 3 (left) shows SST from solution BR (T_1) and Figure 3 (right) shows SST from Comprehensive Ocean-Atmosphere Data Set (COADS) data (T_m) during January, April, July, and October. Except for a few locations, T_1 generally agrees well with T_m with an error < 0.5°C. Along the Somali and Omani coasts, however, T_1 is more than 2°C colder than the observations during the Southwest Monsoon and is somewhat too warm outside the coastal zone (unshaded regions in the western Arabian Sea in the July panel). These differences are certainly due in part to the COADS data being too smoothed, thereby spreading the narrow upwelling regions offshore. They are also likely due to the large interannual variability, which is not included in our solution forced by the climatological winds. In the northwestern Bay of Bengal T_1 is 1.5°C warmer than T_m during winter and 0.5°–1°C colder during summer. East of the Maldives (near 80°E), T_1 is 0.5°–1°C colder than T_m in January. Finally, the cool water present along the southwest coast of India during the Southwest Monsoon in T_m does not appear in T_1. This difference is likely due to inaccuracies in the FSU winds that force the model since the corresponding solution forced by European Centre for Medium-Range Weather Forecasts (ECMWF) winds (averaged from 1980 to 1988) does have colder water there.

In solution BR, T_2 is always less than T_1, so that there are no temperature inversions anywhere in the ocean. This lack is contrary to the observations, which do exhibit strong temperature inversions in the northern and western Bay of Bengal, especially during winter [*Shetye et al.*, 1996].

3.3. Currents

Figure 4 (left) shows surface currents from solution BR ($\mathbf{v}_1$) and Figure 4 (right) shows surface currents from the *Mariano et al.* [1995] ship drift data set ($\mathbf{v}_m$) during January, May, July, and November. The solution reproduces all the major currents present in the ship drift observations, but in many instances they are considerably weaker than in the observations, as is visually apparent from the larger sizes of the shaded regions in Figure 4 (right). Some, but not all, of these discrepancies are improved when salinity forcings are included.

The zonal currents south of India and Sri Lanka but north of the equator, the westward flowing Northeast Monsoon Current (NMC) and the eastward flowing Southwest Monsoon Current (SMC), are important links between the northeast and northwest Indian Ocean (Figure 4, January and July panels). Both are weak in solution BR, with the NMC being 20–35 cm s^{-1} weaker than the ship drift observatories in the southern bay and south of Sri Lanka (also see Figure 6a, top and middle panels).

In the Bay of Bengal and Arabian Sea the annual variability of the model currents compare favorably with the observations, but current speeds tend to be relatively weak. In the Bay of Bengal, for example, both $\mathbf{v}_1$ and $\mathbf{v}_m$ exhibit an anticyclonic gyre during the spring and a cyclonic circulation during the fall. Consistent with *McCreary et al.* [1996], the solution's East India Coastal Current (EICC) generally agrees well with that of the ship drift data, except during late fall and winter when the model EICC is significantly weaker (Figures 7 and 12 below). Likewise, the solution's WICC is 10–20 cm s^{-1} weaker than the observations during the summer (Figure 8). Currents throughout much of the interior Bay of Bengal and Arabian Sea are also relatively weak throughout most of the year, especially during the Southwest Monsoon, when the winds are strongest. This model/data discrepancy is not improved by salinity forcing, possibly because the model lacks a sufficiently thin surface Ekman layer (as conjectured by MKM) or because the ship drift data have a windage error.

Surface currents in the equatorial Indian Ocean reverse direction four times a year, flowing eastward during spring and fall and westward during winter and summer. The eastward currents are commonly referred to as Wyrtki Jets (WJs). In solution BR the fall WJ is considerably weaker than the observed one in the eastern equatorial ocean. This deficiency is explored in detail

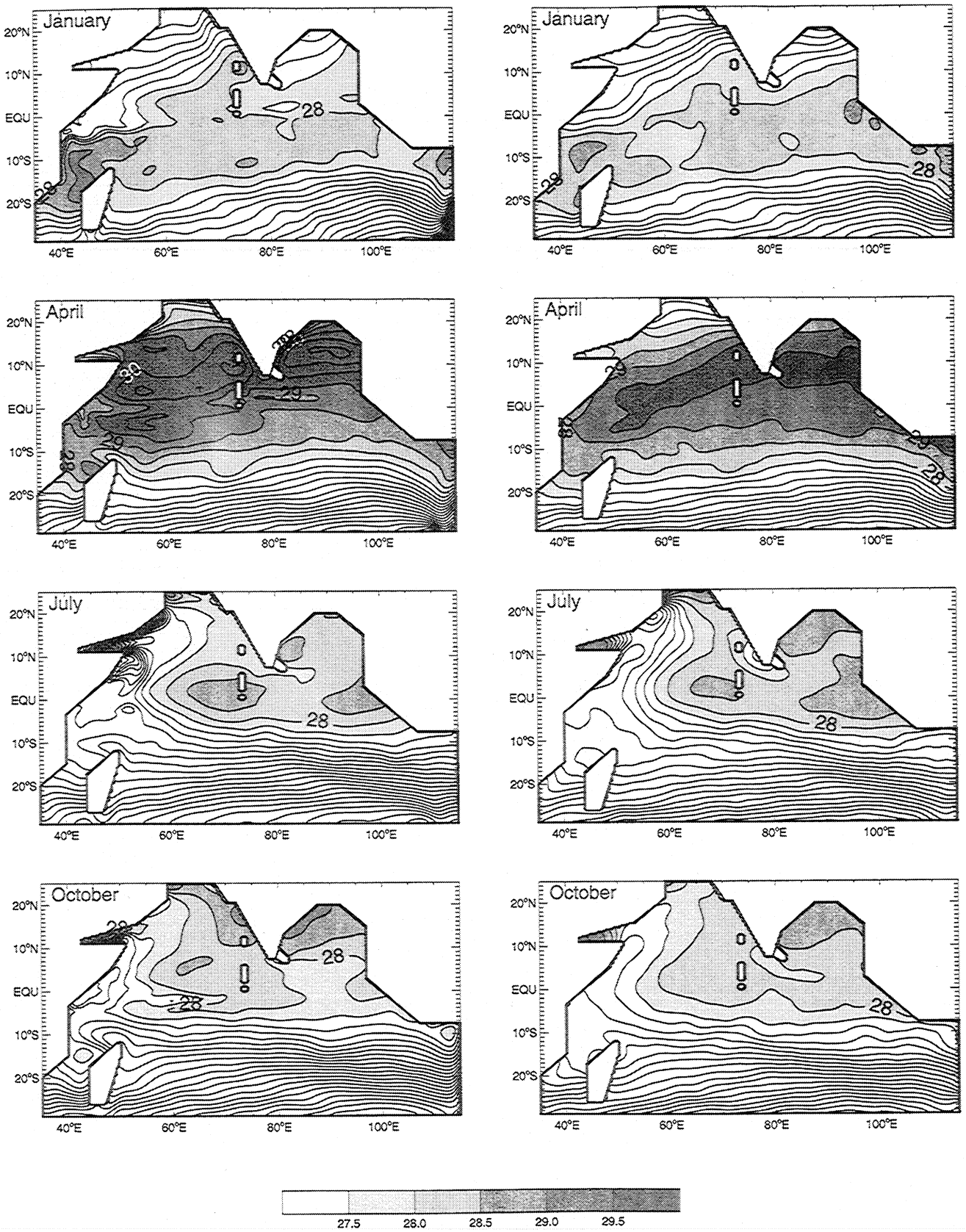

Figure 3. (left) Temperature T_1 from solution BR and (right) corresponding SST T_m from COADS data for January, April, July, and October. The contour interval is 0.5°C. Values > 27.5°C are shaded by the same interval.

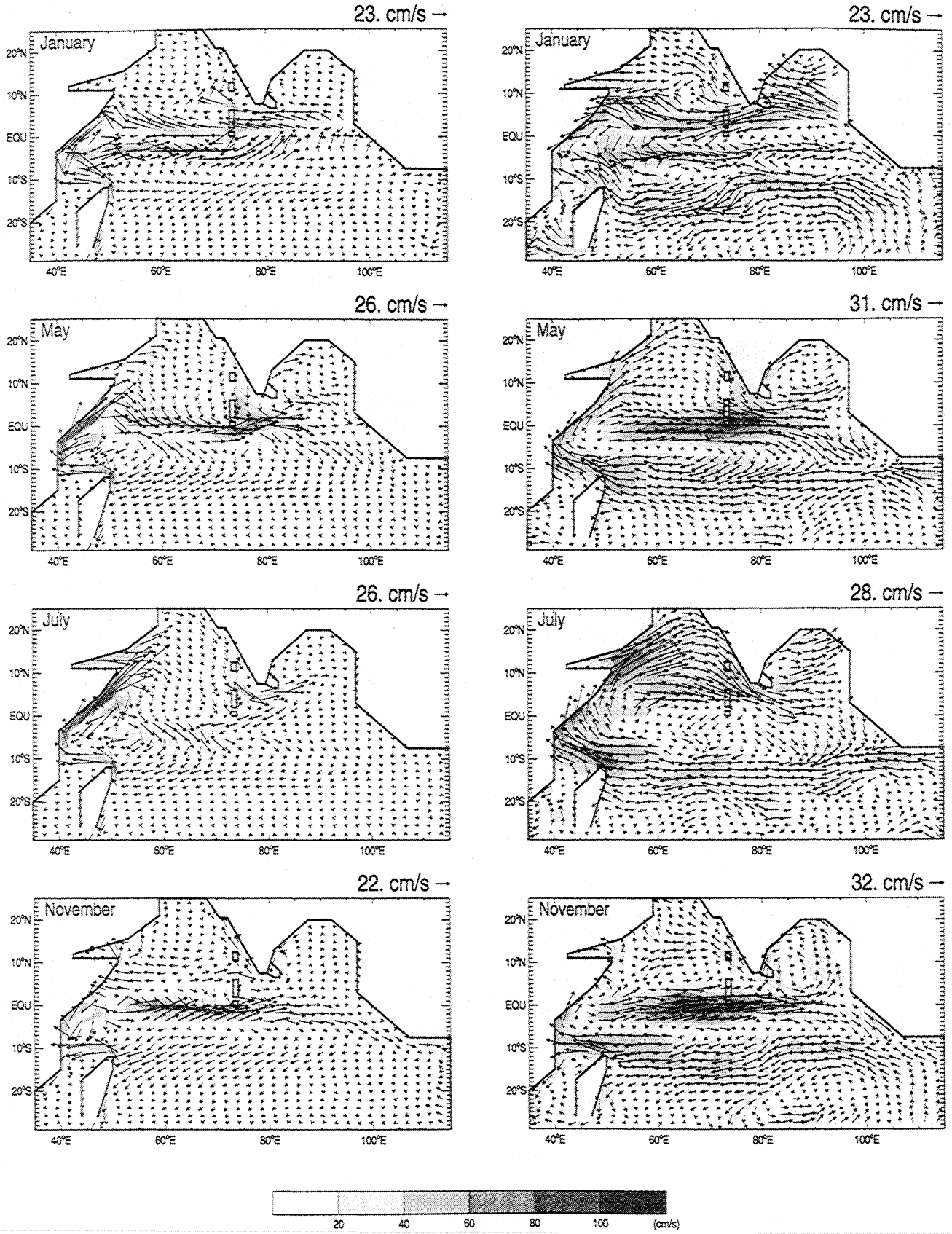

Figure 4. Surface currents (left) from solution BR ($\mathbf{v}_1$) and (right) from ship drift data ($\mathbf{v}_m$) for January, May, July, and November. Shading indicates current amplitudes.

by HMAM, who find that a large part of it results from the lack of precipitation in solution BR.

In solution BR the westward flowing South Equatorial Current (SEC), located at 10–20°S, is also quite weak, especially in the eastern ocean where its speed varies from 0 to 20 cm s^{-1} in comparison to ship drift values of 20–50 cm s^{-1}. As in the Arabian Sea, this error is not improved by salinity forcing. It is also not corrected by including the Indonesian Throughflow: In that case, the SEC is increased by 10–15 cm s^{-1} in the eastern ocean and 5–10 cm s^{-1} in the central and western ocean [see *Han*, 1999, Figure 26a], considerably stronger but still weaker than the ship drift currents. Possible causes of this error again are the model's lack of a sufficiently thin Ekman layer or windage error in the ship drift data.

4. Solution Forced by $\mathcal{P} - \mathcal{E}$

In this section we describe the solution that includes $\mathcal{P} - \mathcal{E}$ forcing by retaining the $\mathcal{P} - \mathcal{E}$ terms in (2b) and in the S_1 equation. This solution is referred to as test run 1 (TR1). The difference solution, TR1 − BR, then measures the influence of $\mathcal{P} - \mathcal{E}$.

4.1. Thicknesses

Forcing by $\mathcal{P} - \mathcal{E}$ generates low salinity in the central and eastern ocean north of 15°S and high salinity in the Arabian Sea and southern tropical ocean [*Han and McCreary*, 2001, Plate 2]. These salinity patterns change the mixed layer thickness by affecting w_k.

Plate 1 (left) shows h_1 differences, Δh_1, from solution TR1 − BR during January, April, July, and October. The most striking feature is that h_1 thins ($\Delta h_1 < 0$) by 10–100 m in a broad region of the central and eastern equatorial ocean (east of 70°E, 7.5°S–7.5°N) during the fall and winter (October and January panels). In addition, h_1 thins by 10–50 m in the eastern bay and by 10–30 m along the west coast of India during July. This thinning is generated by the strong precipitation during summer and fall, which reduces or even reverses the production of turbulent energy P in the mixed layer (equation (2b)) and increases the density jump $\Delta\rho'$ at its bottom (equation (2a)). Both of these effects act to decrease w_k, thereby slowing or reversing entrainment into layer 1.

In contrast, h_1 thickens by 10–30 m in some regions of the northern Arabian Sea during winter (Plate 1 (left), January panel) and by 10–40 m in a large region of the southern tropical ocean and a small region north of Madagascar during July (Plate 1 (left)). This increase results from high evaporation ($\mathcal{P} - \mathcal{E} < 0$), which raises S_1, increases P, and decreases $\Delta\rho'$, and hence strengthens w_k.

Patterns of Δh_2 (Plate 1 (right)) tend to mirror those of Δh_1, with Δh_2 being thicker (thinner) wherever Δh_1 is thinner (thicker). The increase can be large, up to 70 m during October in regions where h_1 is thick and h_2 is close to $h_{2\min}$ in solution BR, whereas h_1 shrinks to $h_{1\min}$ in solution TR1. The resulting h_2 field compares much better with observed estimates of barrier layer thickness (P. Webster et al., manuscript in preparation, 2001).

4.2. Temperatures

4.2.1. Mixed layer. Plate 2 (left) shows the ΔT_1 field from TR1 − BR. In the interior ocean, regions of significant T_1 increase ($\Delta T_1 > 0.1$°C) occur in the central and eastern equatorial ocean during winter, in the equatorial ocean during spring, and to the west of Sumatra during summer. In coastal regions, T_1 increases along the west coast of India during spring, along the west coast of Australia during winter and spring, and in the Gulf of Aden in July. Regions of significant T_1 decrease ($\Delta T_1 < -0.1$°C) include the large area south of the Maldives during fall, the northern Arabian Sea and the eastern ocean near 5°S during winter, and the area north of Madagascar and near the southern boundary during summer. Layer 1 temperatures decrease by more than 1°C along the east African coast in January and near the west coast of Sumatra in October.

According to (4b), changes of T_1 are determined primarily by three processes: entrainment cooling ($E_{T1} \equiv w_1^+(T_1 - T_2)/h_1$), surface heating ($Q_1/h_1$), and advection ($A_{T1} \equiv -\mathbf{v}_1 \cdot \nabla T_1$). Salinity effects forced by $\mathcal{P} - \mathcal{E}$ can alter any of these processes, but most of the aforementioned changes result from changes in entrainment cooling, ΔE_{T1}.

In the interior ocean, significantly warmer T_1 results primarily from decreased entrainment cooling E_{T1} due to the "barrier layer effect." Specifically, lower S_1 due to strong precipitation decreases h_1 and thickens h_2 and thereby increases T_2 markedly (Plate 2 (right); section 4.2.2). The resulting decrease in $T_1 - T_2$ weakens E_{T1}.

Along coasts, T_1 increases are also caused by decreased E_{T1} but directly through a decrease in w_k (and hence w_1^+) rather than through a decrease in $T_1 - T_2$. Along the west coast of India, for example, h_1 is thicker during winter in solution TR1 (Plate 1 (left), January panel) because of increased w_k. As a result, h_1 does not approach its minimum value $h_{1\min}$ in March and April as it does in solution BR. Thus upwelling of cooler water from layer 2 does not occur in TR1, whereas it does occur in BR in order to keep $h_1 = h_{1\min}$. Layer 1 temperatures increase in other coastal regions for the same reason.

The cooling south of the Maldives during October and along the east coast of Africa during January results from increased E_{T1} because of increased upwelling of cool layer 2 water in solution TR1. There is upwelling in both regions, driven by negative wind curl in the former case (see MKM) and by alongshore winds in the latter. In solution BR, h_1 never thins to $h_{1\min}$ in either region.

In solution TR1, however, precipitation increases $\Delta\rho'$ and decreases w_k, so that upwelling favorable winds are able to thin h_1 to $h_{1\min}$; therefore colder layer 2 water must be upwelled into layer 1 to keep $h_1 = h_{1\min}$.

Although T_1 changes are dominated by ΔE_{T1}, they are also affected by other processes. The surface heating anomaly $\Delta(Q_1/h_1)$ caused by $\mathcal{P} - \mathcal{E}$ (not shown) generally has a structure like that of ΔT_1 but with an opposite sign. This inverse relationship happens because T_1 is the only variable that can alter the surface heat flux Q_1 when all other atmospheric variables are kept fixed (as is the case in our model): Lower (higher) T_1 decreases (increases) the latent heat flux Q_e so as to increase (decrease) Q_1, and this process almost always determines $\Delta(Q_1/h_1)$. An exception is along the west coast of India in July, where $\Delta Q_1 > 0$ and $\Delta T_1 < 0$ as expected but $\Delta(Q_1/h_1)$ is, nevertheless, negative. This happens because $Q_1 < 0$ in both solutions but h_1 is considerably thinner in solution TR1; therefore $\Delta(Q_1/h_1)$ is negative even though ΔQ_1 is positive. (In all the solutions in this study, changes in the amount of penetrating radiation due to Δh_1 also affect $\Delta(Q_1/h_1)$, but this process is of secondary importance, weaker by an order of magnitude than the ones noted above.) Advection helps to spread the anomalous temperature regions somewhat, particularly the region of cold T_1 south of the Maldives during October.

4.2.2. Barrier layer. Temperature changes in layer 2 can be much larger than in layer 1, with T_2 varying by as much as 5°C in magnitude (Plate 2 (right)). The large changes are "artificial," however, in the sense that they occur when $h_2 = h_{2\min}$ in one solution (in which case, layer 2 essentially vanishes and is better regarded as part of layer 3) but not in the other. For example, $h_2 = h_{2\min}$ in solution BR in the central and eastern equatorial ocean, so that the barrier layer does not exist in this solution; however, in solution TR1 $h_2 > h_{2\ \min}$, representing the formation of barrier layer due to the strong precipitation. Changes in T_2 result from three major processes (equation (4b)): entrainment cooling when $h_2 = h_{2\min}$ ($E_{T2} \equiv w_2^+ (T_2 - T_e)/h_2$), detrainment heating ($D_{T2} \equiv w_1^- (T_2 - T_1)/h_2$), and advection ($A_{T2} \equiv -\mathbf{v}_2 \cdot \nabla T_2$), and they are mostly determined by ΔE_{T2}.

Temperature T_2 warms most strongly at places where h_1 thins and h_2 becomes thicker than $h_{2\min}$ (compare Plate 1 and Plate 2 (right)). In these regions, T_2 is close to T_e because of entrainment from layer 3 in solution BR. In solution TR1, however, there is a barrier layer ($h_2 > h_{2\min}$), layer 2 no longer entrains cooler water from layer 3, and $E_{T2} \equiv 0$.

Conversely, T_2 cools primarily in areas where $\mathcal{P} - \mathcal{E} > 0$, which increases P and decreases $\Delta\rho'$ in w_k, thickens h_1 until $h_2 = h_{2\min}$, allows layer 2 to entrain cool water from layer 3, and hence makes $E_{T2} > 0$. Prominent regions where this cooling process occurs are the Arabian Sea during January and July, the southern tropical ocean during July, and the southwestern Bay of Bengal during July.

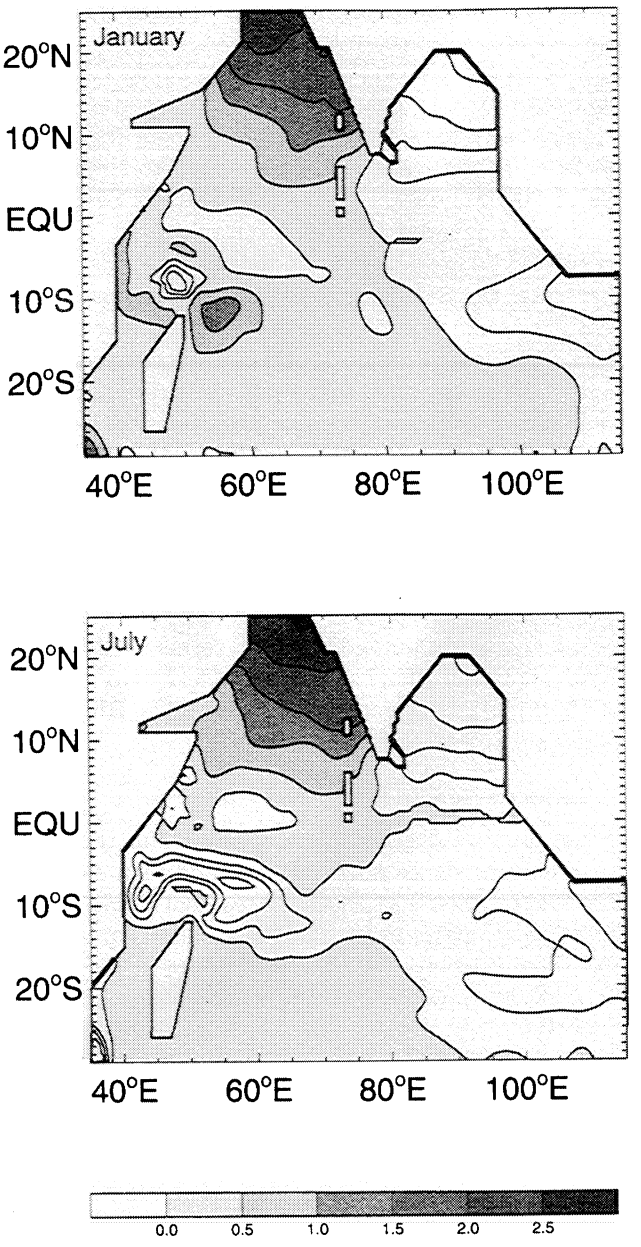

Figure 5. Temperature difference ΔT_3 from solution TR1 – BR during January and July. The contour interval is 0.5°C. Positive values are also shaded with the same interval.

Anomalous detrainment of warmer layer 1 water into layer 2 ($\Delta D_{T2} > 0$) also helps to increase T_2 in regions where high precipitation causes P and w_1 to reverse sign from positive to negative, so that h_1 thins and more warm upper layer water detrains into layer 2. An example is the region of warm ΔT_2 east of the Maldives just north of the equator in July. Advection helps to spread anomalous T_2 regions, an example being the westward stretching of the region of positive ΔT_2 from the southwest coast of India during January.

Temperature inversions ($T_2 > T_1$) can occur in solution TR1 in regions where a barrier layer forms. Regions with temperature inversions are the eastern Bay of Bengal during both Northeast and Southwest Monsoons and the equatorial ocean near 80°E during the Northeast Monsoon (see the discussion of Figure 11 below). These inversions are not present in the *Levitus and Boyer* [1994] data (as measured by $T_{30m}-T_{10m}$ and $T_{50m}-T_{10m}$ fields), but the data may be too sparse and highly averaged to resolve them.

4.2.3. Thermocline layer. Interestingly, although $\mathcal{P}-\mathcal{E}$ is a surface forcing, it can generate large temperature changes in layer 3 (Figure 5). For example, T_3 is 0.5°–2°C warmer in the northern Arabian Sea, 0.5°–2.5°C colder in the Bay of Bengal and near the Lombok Straits, and 0.5°–1.5°C colder north of Madagascar during July. According to (4b), T_3 is influenced by three major processes: subduction heating ($S_{T3} \equiv -w_2^-(T_2 - T_3)/h_3$), cooling due to the entrainment of warmer upper thermocline waters into layer 2 ($E'_{T3} \equiv w_2^+(T_e - T_3)/h_3$), and advection ($A_{T3} \equiv -\mathbf{v}_3 \cdot \nabla T_3$).

In the Arabian Sea, warming of T_3 results mostly from increased subduction of warmer layer 2 water ($\Delta S_{T3} > 0$). During the winter, h_1 (and h_1+h_2 because $h_2 = h_{2\min}$) is thicker in solution TR1 in the northern Arabian Sea because of strengthened entrainment w_k (Plate 1 (left), January panel). Consequently, the subduction rate $w_2^- = w_s$ is larger during the spring, and S_{T3} increases. The warming northeast of Madagascar in January and the relatively weak warming throughout the southern tropical ocean also result from this process.

In contrast, cooling of T_3 in the Bay of Bengal and in the southeastern ocean near 5°–20°S is due primarily to decreased subduction in TR1 ($\Delta S_{T3} < 0$). In the northern bay, for example, the reduction happens because h_1 (and $h_1 + h_2$) thickens much less during the winter in solution TR1 (Plate 1 (left), January panel), so that w_s is weaker during the spring.

The band of negative ΔT_3 north of Madagascar during July is the most prominent region cooled by E'_{T3}. In this region the excess of evaporation over precipitation increases w_k and thickens h_1 (Plate 1 (left), October panel). Because $h_2 = h_{2\min}$ in TR1, the waters that entrain into layer 1 originate from layer 3, and hence $\Delta E'_{T3}$ is large. For a similar reason a negative ΔT_3 forms in a small region north of Madagascar during January.

Advection helps to spread the T_3 anomalies. This process is especially active north of Madagascar (Figure 5, July), where currents are relatively strong [see *Han*, 1999, Figure 8c].

4.3. Currents

The largest surface current change caused by $\mathcal{P}-\mathcal{E}$ is for the fall WJ, which is strengthened by 10–30 cm s^{-1}. The processes that influence the WJs are studied by HMAM. Here then we discuss the other major currents that are influenced by $\mathcal{P}-\mathcal{E}$, namely, the NMC, the EICC, and the WICC.

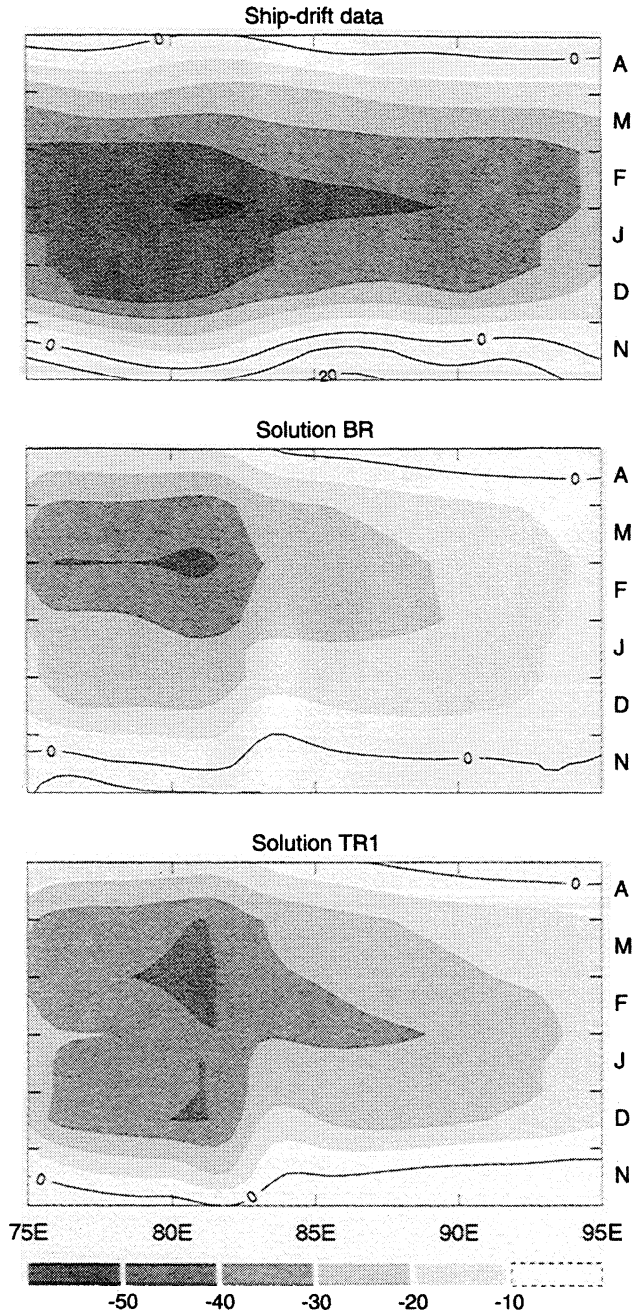

Figure 6a. Longitude-time plots of zonal surface currents averaged from 4.5° to 5.5°N determined from (top) ship drift data U (prepared by *Mariano et al.* [1995]), (middle) solution BR u_1, and (bottom) solution TR1 u_1. Westward currents are shaded, and eastward currents are contoured, with an interval of 10 cm s^{-1}.

Figure 6a shows longitude-time plots of the zonal surface currents averaged from 4.5° to 5.5°N for (top) the ship drift data, (middle) solution BR, and (bottom) solution TR1. By including $\mathcal{P}-\mathcal{E}$ forcing the NMC strengthens by 10–15 cm s^{-1} from November to Jan-

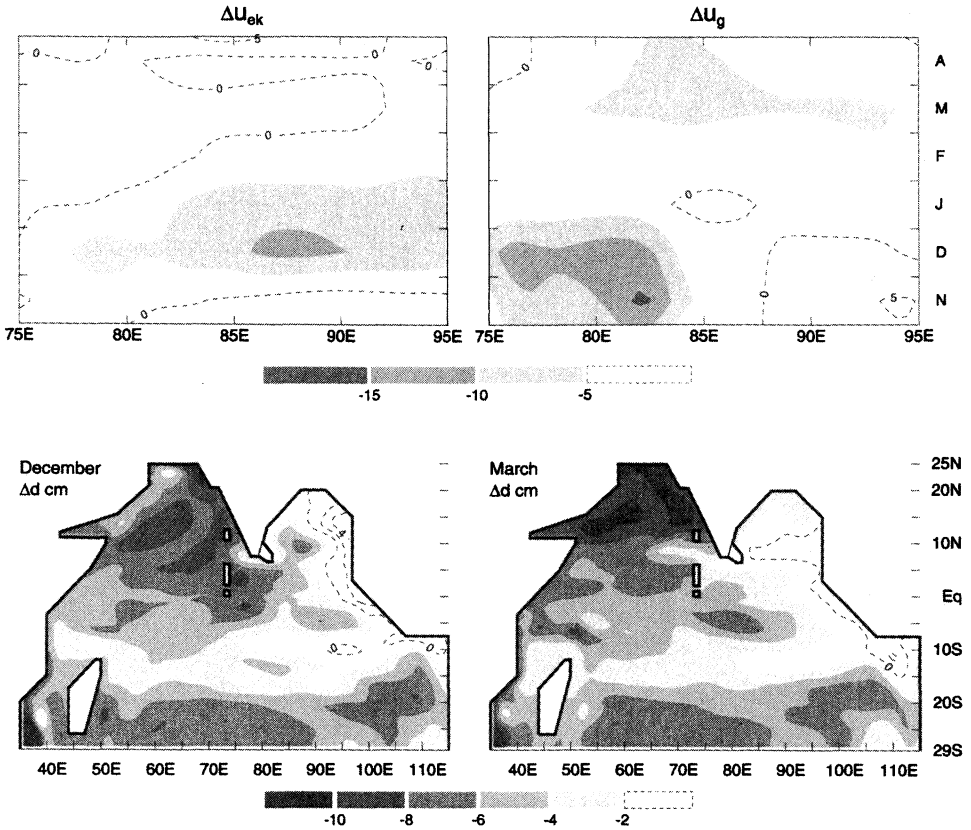

Figure 6b. Longitude-time plots of (top left) zonal Ekman drift (Δu_{ek}) and (top right) zonal geostrophic current (Δu_g), and (bottom) x-y plots of sea level during December and March (Δd) from the difference solution TR1 − BR. Negative values are shaded, and positive values are contoured. The contour interval for currents is 5 cm s^{-1} and that for sea level is 2 cm.

uary, in better agreement with the observations. To illustrate the causes of this improvement, Figure 6b plots velocity differences from TR1 − BR, showing changes in (top left) zonal Ekman drift u_{ek} (equation (8)) and (top right) zonal geostrophic current u_g (equation (9)) and (bottom) sea level d (equation (7)) during December and March.

The strengthened NMC in the southeastern bay (east of 80°E) from December to January results from the increased Ekman drift, which has an amplitude of about 10 cm s^{-1} (Figure 6b (top left)). This stronger Ekman drift is caused by the thinning of h_1 in TR1 due to the strong precipitation during summer and fall (see section 4.1). Near the southern tip of India (75°–80°E) the strengthened NMC is due to the increased geostrophic current (Figure 6b (top right)), which is generated by the anomalous sea level gradient there (Figure 6b (bottom)). In solution TR1, strong precipitation in the northern and eastern bay reduces S_1 and S_2, increasing the density differences $\rho_d - \rho_1$ and $\rho_d - \rho_2$ and therefore d; conversely, strong evaporation in the Arabian Sea generates salty water, decreasing d (Figure 6b (bottom)). Fresher Bay of Bengal water associated with higher sea level is carried to the southern tip of India by the southward EICC during fall and winter, and saltier Arabian Sea Water (ASW) associated with low sea level flows to the eastern ocean via the SMC and the fall WJ. These two water masses meet near the southern tip of India, intensifying the southward meridional pressure gradient force (Figure 6b (bottom left)).

Figure 7 (top) shows EICC velocities at 8°N from the ship drift data (thin curve), solutions BR and TR1 (medium and thick curves), and Ekman drift and geostrophic contributions from solution TR1 − BR (thin and thick dashed curves). Each is the average alongshore current from the Sri Lankan coast to 1.5° offshore. Figure 7 (bottom) shows the sea level anomaly from the difference solution TR1 − BR during September, when the EICC is most strongly affected by $\mathcal{P} - \mathcal{E}$. Forcing by $\mathcal{P} - \mathcal{E}$ causes more than a 10 cm s^{-1} change in the EICC along the Sri Lankan coast during summer and fall, making it agree well with the ship drift data. This improvement results primarily from an increased southward geostrophic current (Figure 7 (top), thick dashed curve); it is caused by the region of low sea level anomaly off the east coast of Sri Lanka increasing the eastward pressure gradient force near the Sri Lankan coast (Figure 7 (bottom)), and this anomalous low sea level results from salty ASW being advected into the bay by the SMC.

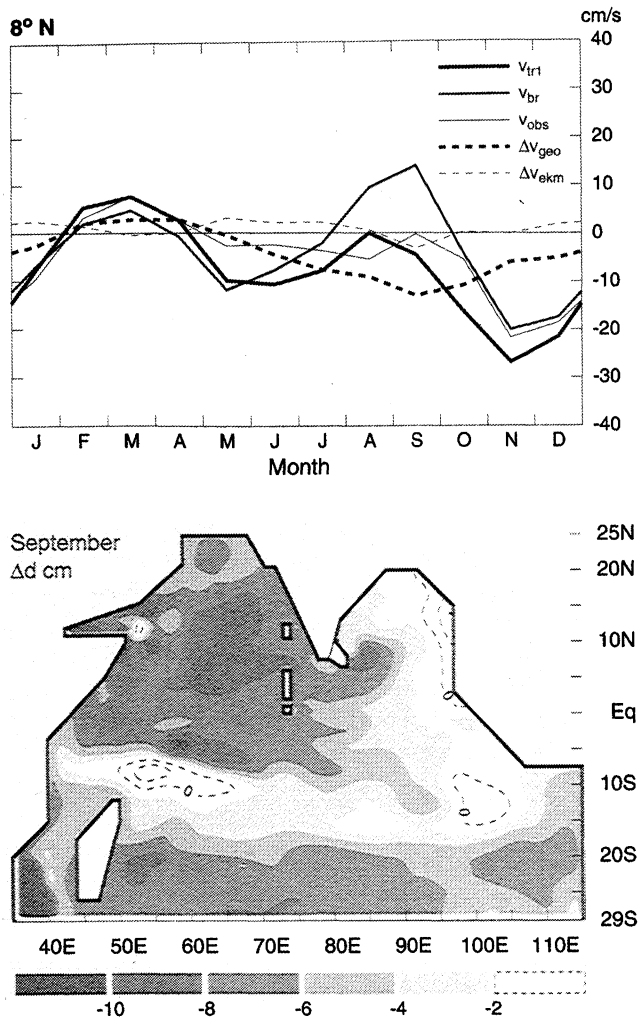

Figure 7. (top) Line plots of the EICC (alongshore surface flow averaged from the coast 1.5° offshore) at 8°N ($\mathrm{cm\,s^{-1}}$) from ship drift data (thin curve), solution BR (medium curve), solution TR1 (thick curve), and the anomalous geostrophic current as well as Ekman drift from TR1 − BR (thick and thin dashed curves). (bottom) An x-y plot of sea level differences from TR1 − BR during September (cm), when the EICC is affected the most by $\mathcal{P} - \mathcal{E}$. Contour labels are the same as those in Figure 6b for Δd.

In solution BR the southward WICC is considerably weaker than the ship drift data during summer, whereas in TR1 it is stronger by 10–20 $\mathrm{cm\,s^{-1}}$ along most parts of the west Indian coast, in much better agreement with the observations (Figure 8 (top) and Figure 8 (middle)). This striking improvement is generated by enhanced Ekman drift (dashed curve) because of h_1 being shallower in TR1 (see section 4.1). Along the southwest coast of India at 8°N (Figure 8 (bottom)), however, the WICC is strongly southward in the data but weak in both solutions. This large discrepancy likely happens because there are insufficient ship drift observations in the region. As a result, the ship drift data (Figure 4) completely miss the Lakshadweep Low, a cyclonic circulation that exists off the southwest coast of India during this season [*Shankar and Shetye*, 1997], resulting in an unrealistically strong southward current at this latitude.

5. Solution Forced by $\mathcal{P} - \mathcal{E}$ and River Inflow

In this section we describe a solution that includes forcing by both $\mathcal{P} - \mathcal{E}$ and river inflow in the Bay of Bengal (solution TR2C). The rivers include the Ganges-Brahmaputra in the northern bay, the Irrawaddy in

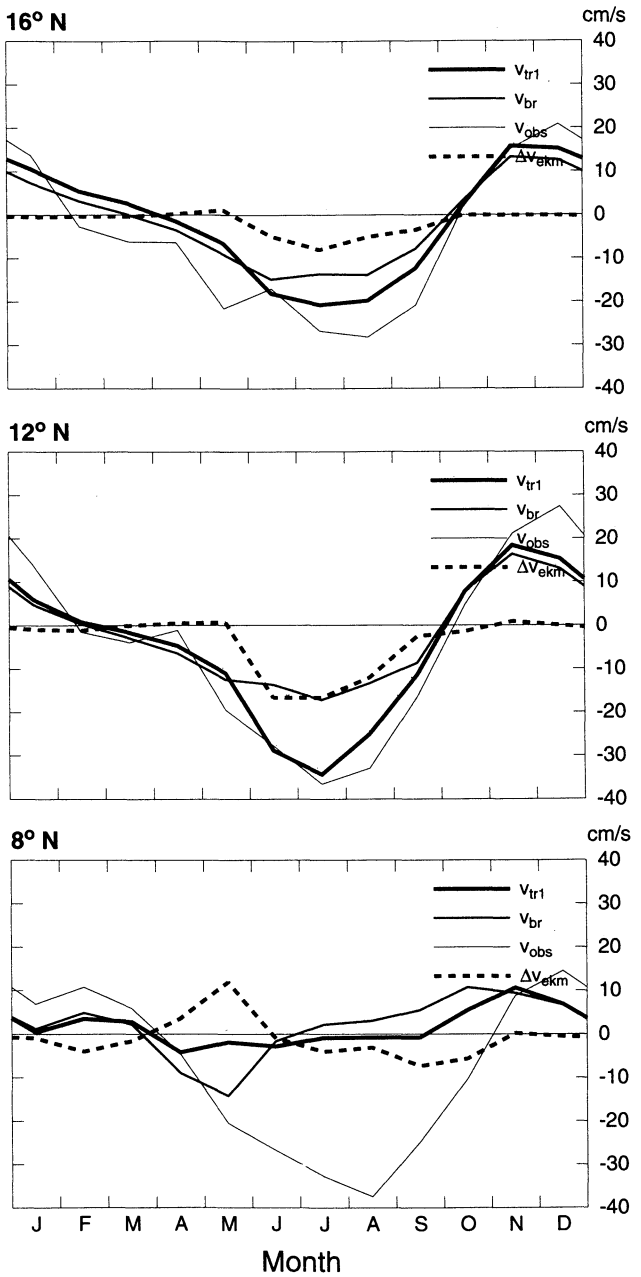

Figure 8. Line plots of the WICC (alongshore surface flow averaged from the coast 1.5° offshore) at (top) 16°, (middle) 12°, and (bottom) 8°N from ship drift data (thin curves), solution BR (medium curves), solution TR1 (thick curves), and Ekman drift difference from TR1 − BR (dashed curves).

the northeastern bay, and a number of smaller rivers along the east coast of India. The rivers are included in the model as exchange flows across basin boundaries within layers 1 and 2, and layer-1 flow is allowed to pass through the shallow channel between Sri Lanka and India [*Han*, 1999; *Han and McCreary*, 2001]. To help isolate river effects, we also recalculated solution TR1 with an open India-Sri Lanka separation in layer 1 (solution TR1′). The difference solution, TR2C – TR1′, then measures effects due only to the rivers.

5.1. Thicknesses

5.1.1. Mixed layer. Plate 3 (left) shows h_1 changes (Δh_1) from the difference solution TR2C – TR1′ during January and July. The most striking changes occur in the northern and western bay during January and in the southern bay and west of the Maldives during July, where h_1 thins by 10–50 m. The thinner h_1 field during January (Plate 3 (top left)) result from decreased entrainment by w_k owing to the decrease in $\Delta\rho'$ caused by the fresher river water being advected into these regions. The decreases in h_1 during July, as well as the narrow band of thinning along the east coast of India, are also caused by this process (Plate 3 (bottom left)).

Curiously, h_1 increases by 10–40 m in the southern bay during January (Plate 3 (top left)). This h_1 increase is produced by an increase in w_k due to decreased $\Delta\rho'$. Fresher water is carried down to 5°N in layer 2 by the southward current in the eastern bay during December and January, but it is confined north of 5°N by the NMC in layer 1 (Figure 4). Thus layer 2 freshens more than layer 1 does south of 5°N, decreasing $\Delta\rho'$ there.

The h_1 field thickens somewhat near the northeast coast of India beginning in July (Plate 3 (bottom left)), and it thickens by more than 10 m there in September (not shown). This h_1 increase is a dynamical adjustment to the mass transport of the exchange flow across the mouth of the Ganges-Brahmaputra River. Specifically, coastal Kelvin waves propagate across the river mouth, adjust the across-boundary flow field to geostrophic balance, and thicken h_1 west of the river mouth. Because the boundary exchange is confined to layers 1 and 2, the excited Kelvin waves are primarily mode-4 waves, which involve upper ocean motions essentially restricted to vertical displacements of h_1 in which $h_1 + h_2 \approx 0$ [*Han*, 1999; HMAM]. These waves cannot propagate very far southwestward along the Indian coast because they are quickly damped by entrainment and detrainment processes. As we shall see below, however, this region of thicker h_1 suppresses coastal upwelling and increases local SST.

The h_1 field of solution TR2C is now much improved over that of solution BR: It shallows markedly during summer and fall in the equatorial ocean because

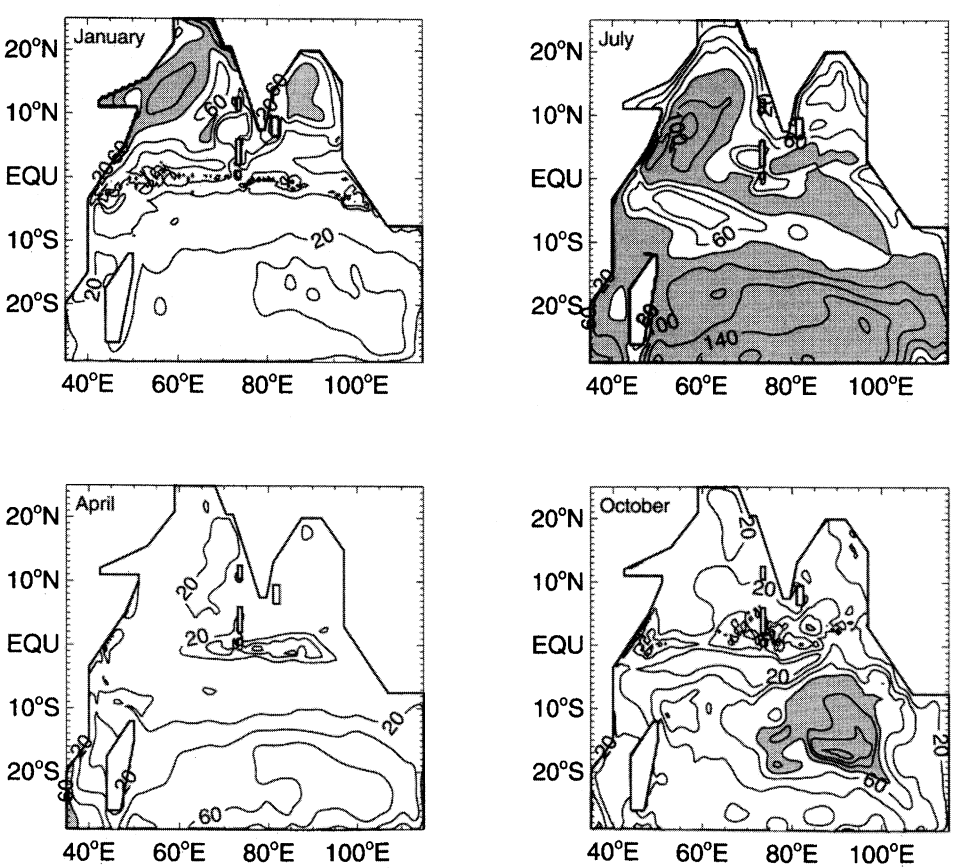

Figure 9. Thickness h_1 from solution TR2C for January, April, July, and October. The contour interval is 20 m. Values > 80 m are shaded.

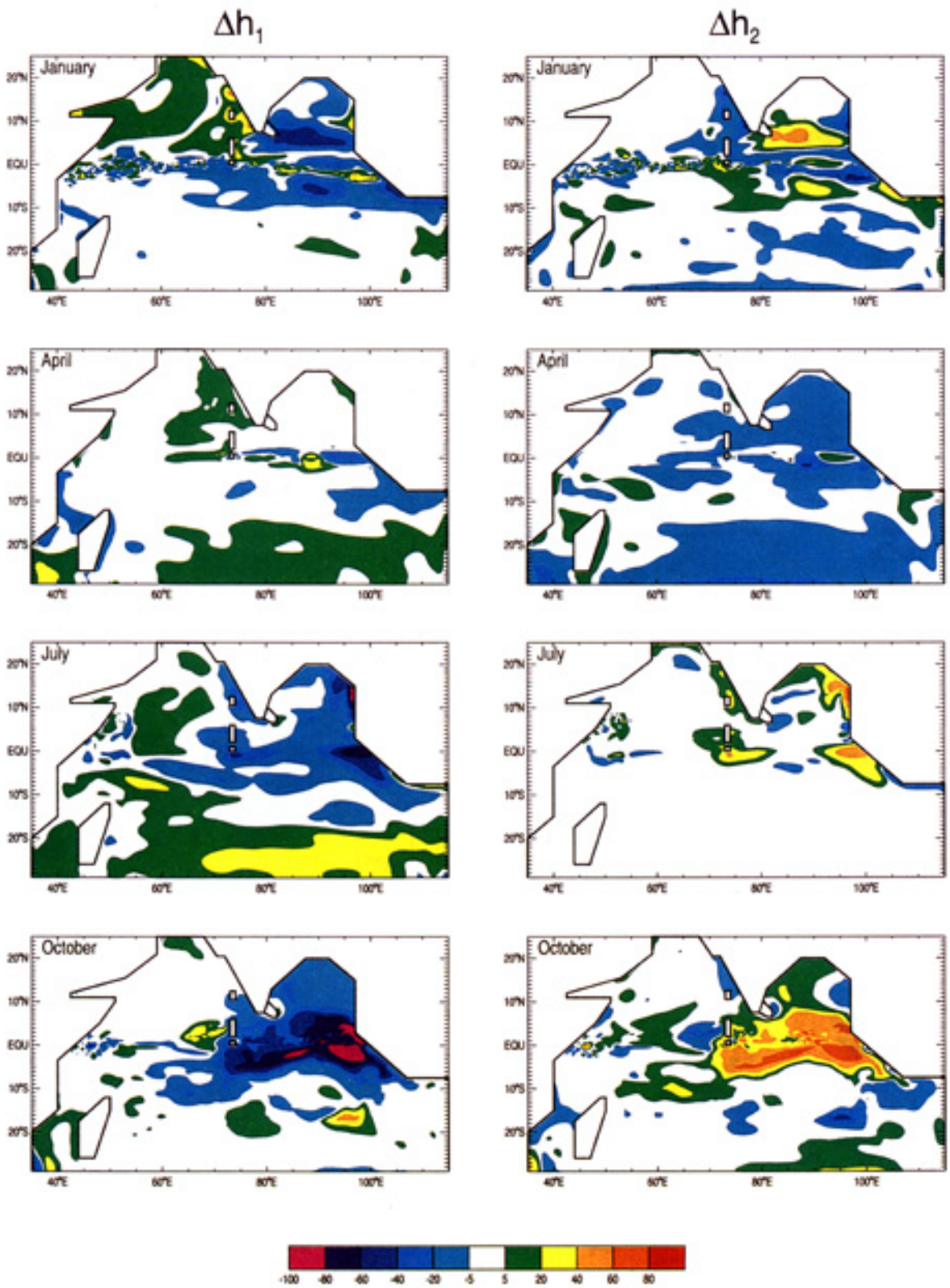

Plate 1. Thickness differences for layers 1 and 2, (left) Δh_1 and (right) Δh_2, from solution TR1 − BR for January, April, July, and October. The unit of the color scale is meters.

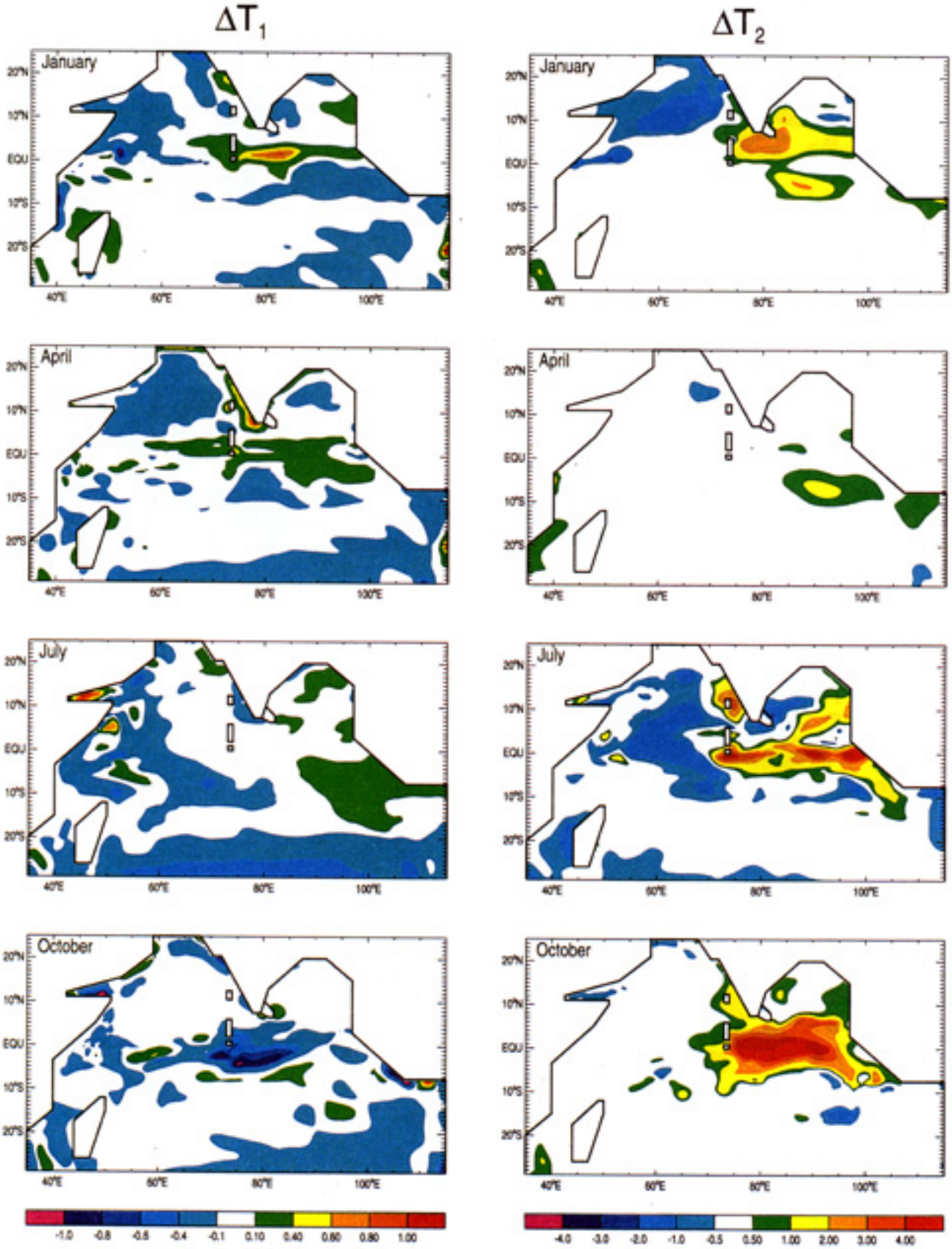

Plate 2. As in Plate 1, except for (left) ΔT_1 and (right) ΔT_2. The unit of the color scale is °C.

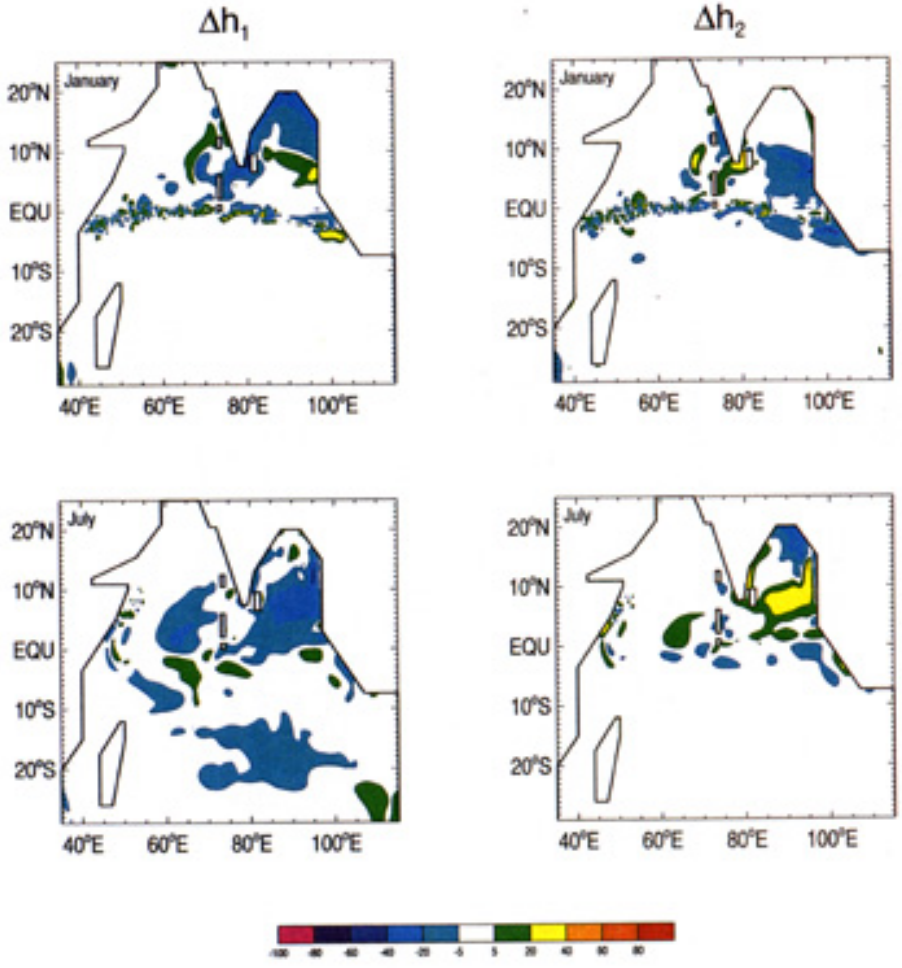

Plate 3. Layer thickness differences, (left) Δh_1 and (right) Δh_2, during January and July from solution TR2C – TR1′. The unit of the color scale is meters.

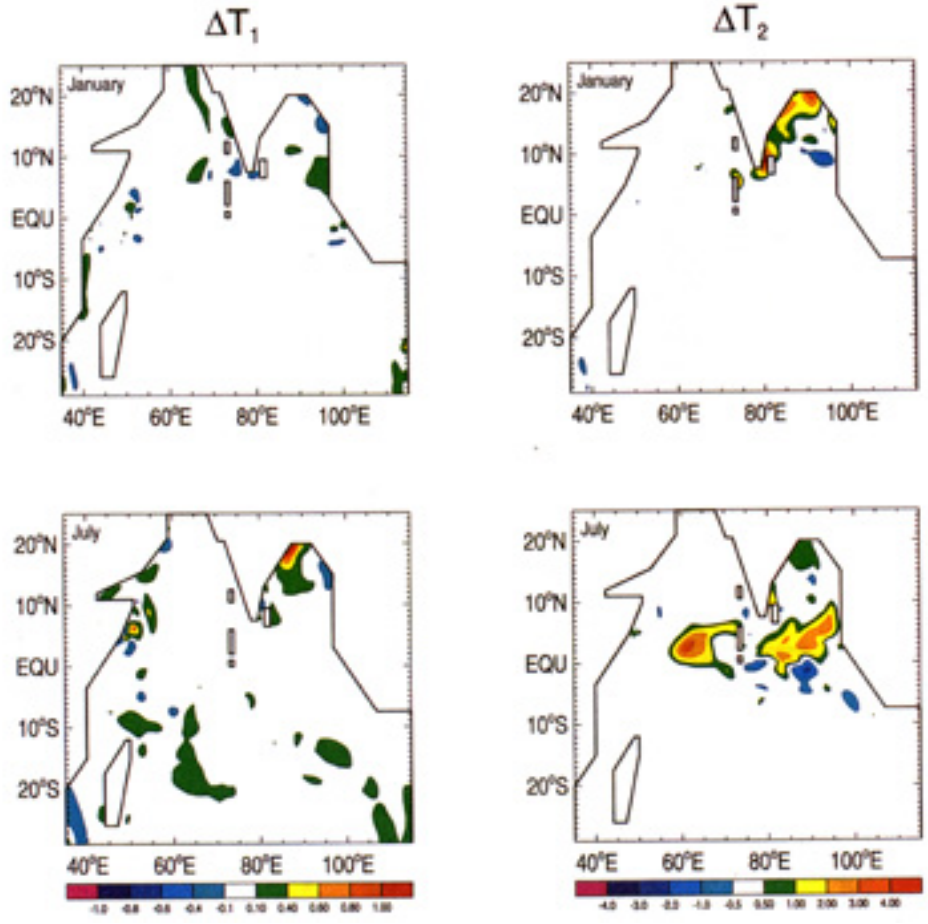

Plate 4. As in Plate 3 except for temperature differences (left) ΔT_1 and (right) ΔT_2. The unit of the color scale is °C.

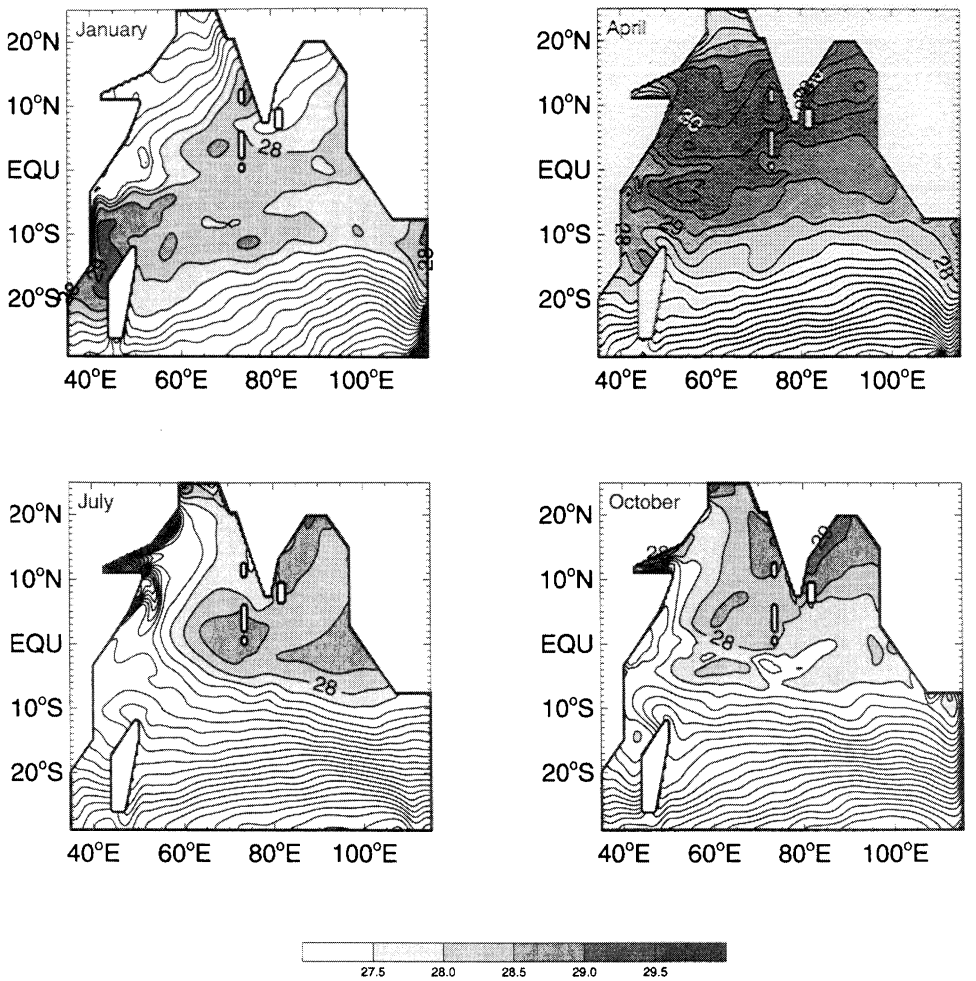

Figure 10. Temperature T_1 from solution TR2C for January, April, July, and October. Labels are the same as those in Figure 3.

of $\mathcal{P} - \mathcal{E}$ and during winter in the northern and western bay because of the rivers (compare Figures 9 and 2). Note, however, that h_1 is still considerably thicker than h_m in the northern Bay of Bengal during winter and in the southern tropical ocean during austral winter, suggesting that our model tends to thicken h_1 too much during wintertime entrainment.

5.1.2. Barrier layer. As for the difference solution TR1 – BR, there are regions where Δh_2 tends to mirror Δh_1. Prominent examples are in the southern Bay of Bengal and along the east coast of India during the Southwest Monsoon, where a barrier layer is formed or strengthened (Plate 3 (bottom)). In the northern bay, however, only one or the other of h_1 and h_2 is significantly affected: During January h_2 stays almost unchanged but h_1 thins by 10–40 m, whereas at other times of the year h_2 is thinner by about 10–30 m and h_1 changes by < 10 m (Plate 3 (top)). This different response happens because h_2 attains its minimum value $h_{2\min}$ owing to entrainment in both TR2C and TR1′ during the winter, so that Δh_2 is relatively small; conversely, during other seasons, h_1 shrinks to its minimum value $h_{1\min}$ and so Δh_1 is small.

5.2. Temperatures

5.2.1. Mixed layer. Plate 4 (left) shows T_1 differences ΔT_1 from solution TR2C – TR1′ during January and July. The most significant T_1 change caused by the rivers occurs in the northwestern bay, where T_1 increases by nearly 1°C during the Southwest Monsoon. This warming results from h_1 being thicker along the northeast Indian coast owing to the mass transport of the Ganges-Brahmaputra, which suppresses coastal upwelling and hence reduces entrainment cooling ($\Delta E_{T1} < 0$). Advection and mixing spread the warmer water somewhat offshore.

During the winter the northern Bay of Bengal is cooled by surface fluxes ($Q_1 < 0$), largely by increased Q_e due to cool dry air blowing off the continent. Surprisingly, then, although h_1 thins by 10–50 m around the perimeter of the bay during the Northeast Monsoon (Plate 3 (top left)), T_1 does not decrease much despite the significant increase in surface cooling rate Q_1/h_1. The reason it does not is because entrainment cooling E_{T1} is weaker since w_k is much less. The decrease in E_{T1} almost compensates for the Q_1/h_1 increase.

In comparison to solution BR, the T_1 field in solution TR2C agrees better with the COADS data in several regions (compare Figures 3 and 10). Regions that are improved by $\mathcal{P} - \mathcal{E}$ forcing are located east of the Maldives in January, along the west coast of India in April, and near and south of the Maldives (near 2°S). The northward push of relatively cold water southeast of the Maldives, however, is somewhat too cold in solution TR2C in comparison with the data. The prominent region improved by river inflow is along the northeast coast of India, where T_1 is warmer by nearly 1°C.

In the northern bay, however, T_1 in solution TR2C is still 1°C warmer than the observations during winter. This model/data discrepancy suggests that cooling processes, not properly represented in our model, are important for cooling SST in the northern bay. The most likely problem is that Q_e is not strong enough in the model, because of high-frequency variability that is not resolved by the monthly mean forcing winds. To model this effect, we allowed the scalar wind to have a minimum speed of 6 m s^{-1} in a test solution (solution TR2D). As expected, T_1 dropped by 1°C during January in the northern bay, bringing T_1 into reasonable agreement with the observations. In most of the interior tropical ocean, however, T_1 is 0.5°–1°C colder than the data, suggesting that specifying a constant minimum wind speed for the entire basin is not appropriate.

5.2.2. Barrier and thermocline layers. As for $\mathcal{P} - \mathcal{E}$ forcing (Plate 2), rivers generate large-amplitude T_2 changes due to decreased entrainment cooling (ΔE_{T2} <0), with T_2 warming by 0.5°–4°C in the northern and western bay throughout the year and in the southern bay and the equatorial ocean during the Southwest Monsoon (Plate 4 (right)).

There are also small-scale regions where T_2 decreases significantly ($\Delta T_2 < -1$°C), such as in the southeastern bay during winter and in the eastern equatorial ocean during summer. The first cooling is caused by an increase in w_k that thins h_2 to $h_{2\min}$ (Plate 3 (top left)), making layer 2 entrain colder water T_e from layer 3 and increasing E_{T2}. The latter is caused by weakened detrainment heating D_{T2} caused either by w_1 switching from detrainment in TR1′ ($w_1 < 0$) to entrainment in TR2C ($w_1 > 0$) or by the Monin-Obukhov depth h_{mo} being thicker in solution TR2C because S_1 is lower at locations where $P < 0$, resulting in less detrainment.

Because of the considerably warmer T_2 and somewhat colder T_1 in solution TR2C near the northwestern boundary of the Bay of Bengal during the Northeast Monsoon, temperature inversions form near the Indian coast in the northwestern bay (Figure 11), consistent with the observations (*Shetye et al.* [1996] and $T_{30m} - T_{10m}$ from *Levitus and Boyer* [1994]). This inversion region does not exist in solution TR1′, which has no river influences. Even in solution TR2C, however, temperature inversions occur only during winter in the northwestern bay, whereas they happen almost throughout the year in the observations [*Shetye et al.*, 1996]. This discrepancy may be because our model describes layer-averaged temperatures so that only the strongest wintertime inversions can be resolved. The inversions in most other regions (central and eastern bay and at some locations in the eastern equatorial ocean) also exist in solution TR1′ and so are due to $\mathcal{P} - \mathcal{E}$ forcing. The rivers strengthen and broaden them, especially in the southern bay. Similar to the $\mathcal{P} - \mathcal{E}$, the Bay of Bengal rivers cause appreciable T_3 changes (figure not shown) in the Bay of Bengal and along the west coast of India because of decreased subduction heating ($\Delta S_{T3} < 0$).

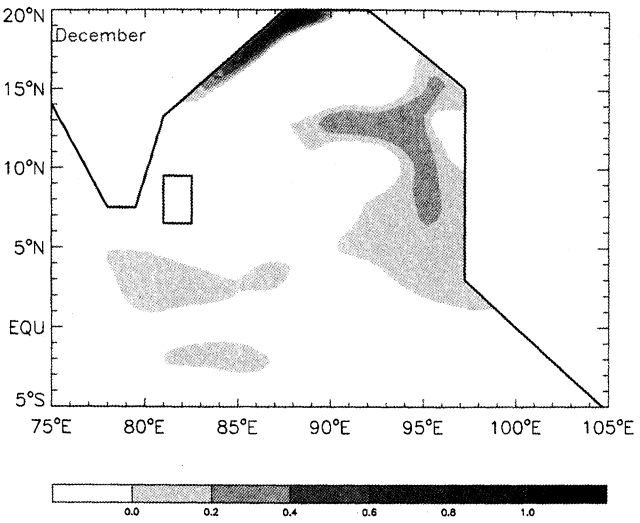

Figure 11. Temperature difference $T_2 - T_1$ from solution TR2C during December, illustrating temperature inversions due to rivers. The shading interval is 0.2°C.

5.3. Currents

The most significant current change caused by the rivers is for the EICC during the Northeast Monsoon, which is strengthened by nearly 10 cm s^{-1} (Figure 12 (top) and Figure 12 (middle)). The wintertime southward EICC [*Shankar et al.*, 1996; *McCreary et al.*, 1996] carries the fresher river water southward along the east coast of India as a coastal plume, increasing coastal sea level and strengthening the across-shelf pressure gradient (Figure 12 (bottom)). As a result, a strip of southwestward geostrophic current is generated (dashed lines of Figures 12 (top) and 12 (middle)). For a similar reason the rivers increase the NMC by 5–10 cm s^{-1} near 7°N in the bay during March (not shown).

In contrast, the WICC is not appreciably strengthened by the flow of fresh water up the west coast of India, in contradiction to the hypothesis of *Shetye et al.* [1996]. This is because the across-shelf sea level gradient along the west coast of India is not increased as much as it is along the east Indian coast.

5.4. Sea Level

Figure 13 shows the annual cycle of sea level (relative to the corresponding annual mean) from solution

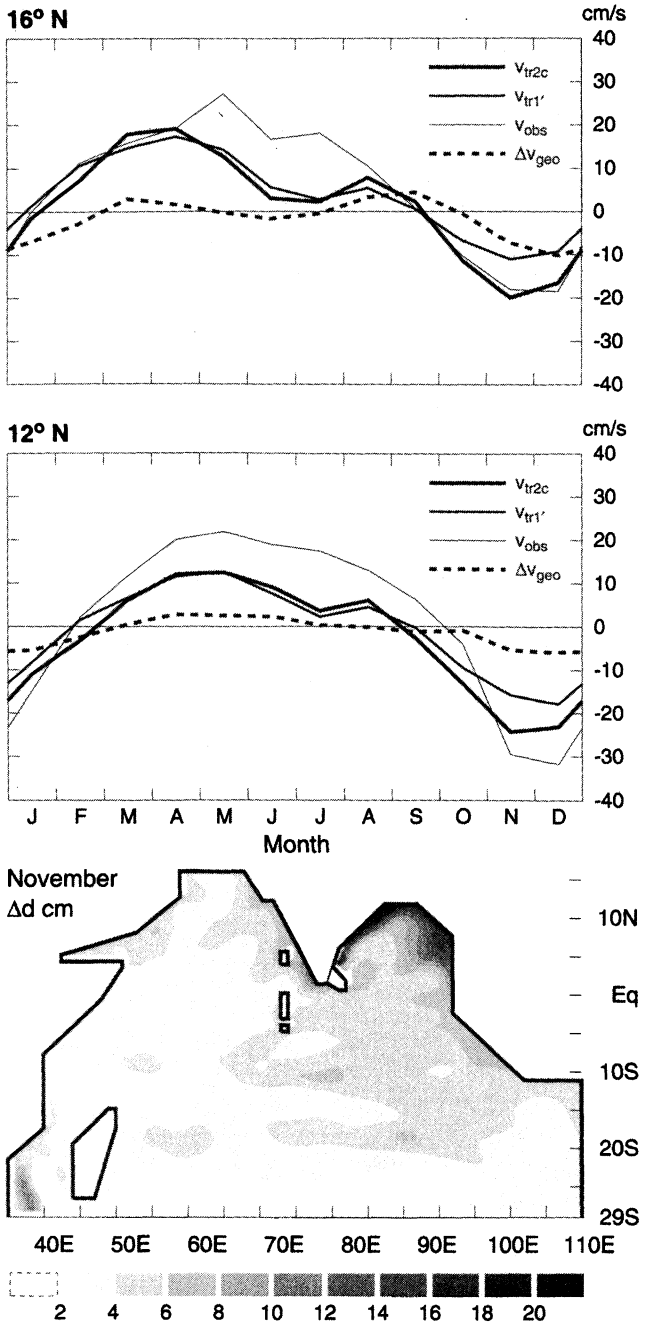

Figure 12. Line plots of the EICC (alongshore surface flow averaged from the coast 1.5° offshore) at (top) 16°N and (middle) 12°N from solution TR2C (thick curve), TR1′ (medium curve), ship drift data (thin curve), and the anomalous geostrophic current caused by the rivers (TR2C − TR1′; dashed curve). (bottom) The sea level anomaly (Δd) during November from difference solution TR2C − TR1′. The contour interval is 2 cm.

TR2C (thick curve), solution TR1 (medium curve), and the observed climatology (thin curve) [after *Shetye and Almeida*, 1985] at Vishakhapatnam (17°N) and Madras (12.5°N). At Vishakhapatnam, fresher river water increases sea level by more than 10 cm during fall and winter and decreases it by more than 5 cm in April (Figure 13 (top)). In a similar way but to a lesser extent, rivers affect sea level at Madras (Figure 13 (bottom)). These changes bring sea level in solution TR2C into much better agreement with the observations.

The reasons for the improvement are as follows. Fresher water from the Ganges-Brahmaputra flows along the east coast of India as a coastal plume during the Northeast Monsoon, and pushes southward in the northern bay during the Southwest Monsoon (*Han and McCreary*, 2001, Plate 3a). It significantly increases $\rho_d - \rho_1$ and $\rho_d - \rho_2$ because of its low salinity, resulting in increased sea level, especially during the Northeast Monsoon (Figure 13). From February to May the western branch of the basin-wide anticyclonic gyre (Figure 4) brings saltier water from the southern bay northward, and sea level is affected the least by rivers during this season. As a consequence of all these effects, the amplitude of the annual sea level oscillation (thick curves) is increased, the large negative signal during April occurring because a larger annual mean has been removed.

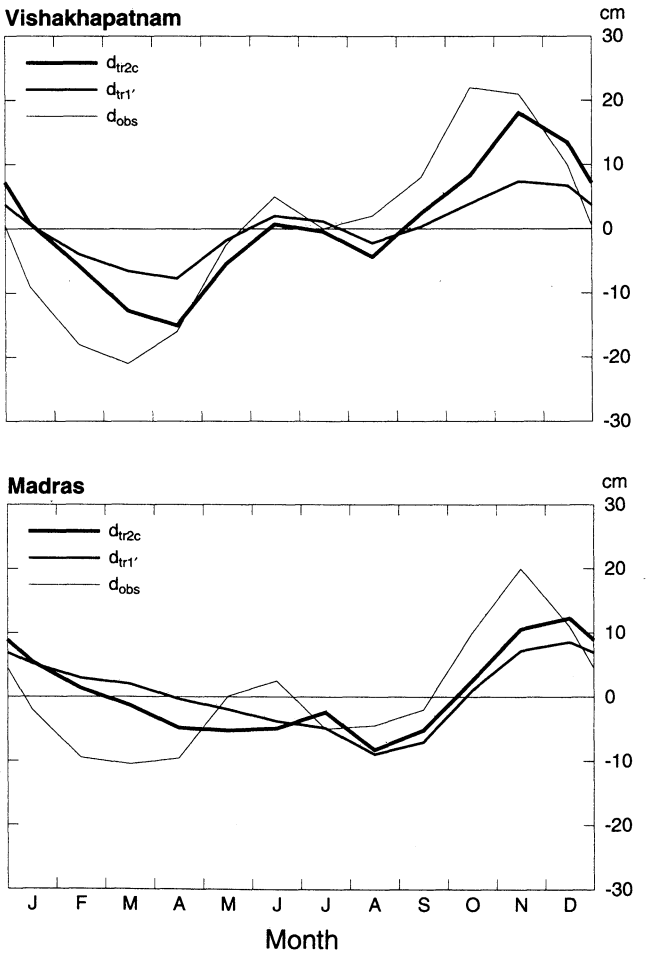

Figure 13. Line plots of sea level from solution TR2C (thick curve), solution TR1′ (medium curve), and climatology (thin curve) [*Shetye and Almeida*, 1985] at stations (top) Vishakhapatnam (17°N) and (bottom) Madras (12.5°N) near the east Indian coast. The plotted curves are total sea level minus their respective annual means.

6. Summary and Conclusions

In this paper, a $4\frac{1}{2}$-layer model is used to examine effects of $\mathcal{P} - \mathcal{E}$ and the Bay of Bengal rivers on mixed layer physics, dynamics, and thermodynamics in the Indian Ocean. Forcing by $\mathcal{P} - \mathcal{E}$ is introduced in the equation for S_1 [*Han and McCreary*, 2001, equation (1)] and in the w_k equation (2a), and rivers are added by specifying boundary fluxes at corresponding locations [see *Han and McCreary*, 2001].

In regions where $\mathcal{P} - \mathcal{E} > 0$ and S_1 is low, such as the central and eastern equatorial ocean during the summer and fall and the west coast of India during the Southwest Monsoon, h_1 shallows and h_2 thickens because of decreased entrainment by w_k, forming a barrier layer (Plate 1). As a result, both T_1 and T_2 increase because entrainment cooling in both layers is weakened (Plate 2), and surface currents increase because h_1 is thinner and so momentum is more surface concentrated (Figures 6a, 6b, and 8). Conversely, in regions where $\mathcal{P} - \mathcal{E} < 0$ and S_1 is high, such as the northern Arabian Sea and a broad region of the southern tropical ocean, h_1 thickens and h_2 thins because of increased entrainment by w_k, resulting in colder T_2 and T_1. Anomalous sea level gradients, which are generated where fresher Bay of Bengal water with high sea level meets saltier ASW with low sea level, enhance the southward EICC east of Sri Lanka and the NMC (Figures 6a, 6b, and 7). In layer 3, T_3 warms in the northern Arabian Sea and cools in the Bay of Bengal as well as southwest of Sumatra because of increased and decreased subduction, respectively (Figure 5).

In regions where significant amounts of river water are present, such as the southern bay during the Southwest Monsoon and near the northern and western boundaries of the bay during the Northeast Monsoon, h_1 thins and h_2 thickens by 10–50 m because of decreased entrainment by w_k, and a barrier layer is either formed or strengthened (Plate 3). As a result of this shallowing, entrainment into both layers decreases, and T_2 increases considerably. In the latter case (northern bay), however, T_1 does not increase because of weakened entrainment cooling, as might be expected, but rather cools somewhat because the thinner h_1 enhances surface cooling (Plate 4). The warm T_2 and somewhat colder T_1 generate temperature inversions in the above regions, especially in the northwestern bay in December (Figure 11). In the northwestern bay, T_1 increases by 1°C during the Southwest Monsoon, when the transport of river Ganges-Brahmaputra approaches its maximum; this significant mass influx forces coastal Kelvin waves associated with a thicker h_1, suppressing coastal upwelling thereby increasing T_1. The freshwater plume during the Northeast Monsoon increases sea level along the east coast of India (Figures 12 and 13), strengthening the southward EICC by 10 cm s^{-1} during winter (Figure 12). For a similar reason the NMC is enhanced by 5–10 cm s^{-1} during March. In layer 3, fresh water from the rivers decreases T_3 by as much as 1°C in the bay because of decreased subduction.

In conclusion, we have isolated the separate influences of forcing by $\mathcal{P} - \mathcal{E}$ and river inflow on mixed layer thicknesses, temperatures, and surface currents in the Indian Ocean. These influences can be large. For example, they cause the mixed layer to thin markedly in the eastern tropical ocean, a change that alters the upper ocean heat content in the region and is therefore likely to be important in climate dynamics. Furthermore, solutions are able to simulate observed fields quite well, and aspects are improved as various salinity forcings are added. There are discrepancies between observed and modeled fields, but they are not severe and tend to be a matter of degree rather than a fundamental misrepresentation. This success is encouraging, suggesting that our model adequately represents the primary physical processes at work in the region.

Acknowledgments. This paper is based on Weiqing Han's thesis work, and she is grateful to the support of her committee members: Richard Dodge, Barry Klinger, Arthur Mariano, Robert Molinari, and Don Olson. We thank S. R. Shetye and D. Shankar for helpful suggestions and discussions. This research was supported by NSF through grants OCE-92-03916 and OCE-94-16098, by ONR through contract N00014-97-1-0077, and by the Frontier Research System for Global Change through its sponsorship of the International Pacific Research Center (IPRC). This manuscript is SOEST Contribution No. 5318 and IPRC Contribution No. 71.

References

Anderson, D. L. T., and D. J. Carrington, Modeling interannual variability in the Indian Ocean using momentum fluxes from the UKMO and ECMWF operational weather analyses, *J. Geophys. Res., 98*, 12,483–12,499, 1993.

Anderson, D. L. T., D. J. Carrington, R. Correy, and C. Gordon, Modeling the variability of the Somali Current, *J. Mar. Res., 49*, 659–696, 1991.

Godfrey, J. S. and T. T. Golding, The Sverdrup relation in the Indian Ocean and the effect of Pacific-Indian Ocean throughflow on Indian Ocean circulation and on the east Australian current, *J. Phys. Oceanogr., 11*, 771-779, 1981.

Godfrey, J. S., and A. J. Weaver, Is the Leeuwin Current driven by Pacific heating and winds?, *Prog. Oceanogr., 27*, 225–272, 1991.

Han, W., Influence of salinity on dynamics, thermodynamics, and mixed-layer physics in the Indian Ocean, Ph.D. dissertation, 147pp., Oceanogr. Cent., Nova Southeastern Univ., Dania, Fl., 1999.

Han, W., and J. P. McCreary, Modeling salinity distribution in the Indian Ocean, *J. Geophys. Res., 106*, 859–877, 2001.

Han, W., J. P. McCreary, D. L. T. Anderson, and A. J. Mariano, On the dynamics of the eastward surface jets in the equatorial Indian Ocean, *J. Phys. Oceanogr., 29*, 2191–2209, 1999.

Hirst, A. C., and J. S. Godfrey, The role of Indonesian Throughflow in a global ocean GCM, *J. Phys. Oceanogr., 23*, 1057-1086, 1993.

Kraus, E. B., and J. S. Turner, A one-dimensional model of the seasonal thermocline, II, The general theory and its consequences, *Tellus, 119*, 98–106, 1967.

Kundu, P. K., and J. P. McCreary, On the dynamics of the throughflow from the Pacific into the Indian Ocean, *J. Phys. Oceanogr., 16*, 2191–2198, 1986.

Legates D. R., and C. J. Willmott, Mean seasonal and spatial variability in gauge-corrected global precipitation, *Int. J. Climatol., 10(2)*, 111–127, 1990.

Legler D. M., I. M. Navon, and J. J. O'Brien, Objective analysis of pseudo-stress over the Indian Ocean using a direct-minimization approach, *Mon. Weather Rev., 117*, 709–720, 1989.

Levitus, S., and T. P. Boyer, *World Ocean Atlas 1994*, vol. 4, Temperature, NOAA Atlas NESDIS 4, 117 pp., Natl. Oceanic and Atmos. Admin., Silver Spring, Md., 1994.

Levitus, S., R. Burgett, and T. P. Boyer, *World Ocean Atlas 1994*, vol. 3, Salinity, NOAA Atlas NESDIS 3, 99 pp., Natl. Oceanic and Atmos. Admin., Silver Spring, Md., 1994.

Lukas R., and E. Lindstrom, The mixed layer of the western equatorial Pacific Ocean, *J. Geophys. Res., 96*, suppl., 3343–3357, 1991.

Mariano, A. J., E. H. Ryan, B. D. Perkins, and S. Smithers, The Mariano global surface velocity analysis 1.0, *USCG Rep.* CG-D-34-95, 55 pp., Res. and Devel. Cent., U. S. Coast Guard, Groton, Conn., 1995.

McCreary, J. P., and P. K. Kundu, A numerical investigation of sea-surface temperature variability in the Arabian Sea, *J. Geophys. Res., 94*, 16,097–16114, 1989.

McCreary, J. P., P. K. Kundu, and R. L. Molinari, A numerical investigation of dynamics, thermodynamics, and mixed-layer processes in the Indian Ocean, *Prog. Oceanogr., 31*, 181–224, 1993. (Erratum, *Prog. Oceanogr., 33*, 248, 1994.)

McCreary, J. P., S. Zhang, and S. R. Shetye, Coastal circulations driven by river outflow in a variable-density $1\frac{1}{2}$-layer model, *J. Geophys. Res., 102*, 15,535–15,554, 1997.

McCreary, J. P., W. Han, D. Shankar, and S. R. Shetye, On the dynamics of the East India Coastal Current, 2, Numerical solutions, *J. Geophys. Res., 101*, 113,993–14,010, 1996.

Murtugudde, R., and A. Busalacchi, Salinity effects in a tropical ocean model, *J. Geophys. Res., 103*, 3283–3300, 1998.

Murtugudde, R., A. Busalacchi, and J. Beauchamp, Seasonal-to-interannual effects of the Indonesian throughflow on the tropical Indo-Pacific Basin, *J. Geophys. Res., 103*, 21,425-21,441, 1998.

Rao, R. R., R. L. Molinari, and J. F. Festa, Evolution of the climatological near-surface thermal structure of the tropical Indian Ocean, part 1, Description of mean monthly mixed-layer depth and sea-surface temperature, surface-current and surface meteorological fields, *J. Geophys. Res., 94*, 10,801–19,815, 1989.

Rao, R. R., R. L. Molinari, and J. F. Festa, Surface meteorological and near-surface oceanographic atlas of the tropical Indian Ocean, *NOAA Tech. Memo.* ERL AOML-69, Natl. Oceanic and Atmos. Admin., Silver Spring, Md., 1991.

Schiller, A., J. S. Godfrey, P. C. McIntosh, G. Meyers, and S. E. Wijffels, Seasonal near-surface dynamics and thermodynamics of the Indian Ocean and Indonesian Throughflow in a global ocean general circulation model, *J. Phys. Oceanogr., 28*, 2288–2312, 1998.

Semtner, A. J., and R. M. Chervin, Ocean general circulation from a global eddy resolving model, *J. Geophys. Res., 97*, 5493–5550, 1992.

Shankar, D., and S. R. Shetye, On the dynamics of the Lakshadweep high and low in the southeastern Arabian Sea, *J. Geophys. Res., 102*, 12,551–12,562, 1997.

Shankar, D., J. P. McCreary, W. Han, and S. R. Shetye, On the dynamics of the East India Coastal Current, part 1, Analytic solutions forced by interior Ekman pumping and local alongshore winds, *J. Geophys. Res., 101*, 13,975–13,991, 1996.

Shetye, S. R., and A. M. Almeida, An examination of the factors that influence the monthly-mean sea level along the coast of India, *IOC Workshop Rep., 37*, pp. 87–104, U. N. Educ., Sci. and Cult. Org., Paris, 1985.

Shetye, S. R., A. D. Gouveia, D. Shankar, S. S. C. Shenoi, P. N. Vinayachandran, D. Sundar, G. S. Michael, and G. Nampoothiri, Hydrography and circulation of the western Bay of Bengal during the Northeast Monsoon, *J. Geophys. Res., 101*, 14,011–14,025, 1996.

Vialard, J., and P. Delecluse, An OGCM study for the TOGA decade, part II, Barrier layer formation and variability, Tech. Rep. 4, Inst. Pierre Simon Laplace, Paris, France, 1998.

Vinayachandran, P. N., The Bay of Bengal circulation in an OGCM, Ph.D. Dissertation, 167pp., Cent. for Atmos. Sci., Indian Inst. of Sci., Bangalore, India, 1995.

Vinayachandran, P. N., Y. Masumoto, T. Mikawa, and T. Yamagata, Intrusion of the Southwest Monsoon Current into the Bay of Bengal, *J. Geophys. Res., 104*, 11,077–11,085, 1999.

Yang, S, K.-M. Lau, and P. S. Schopf, Sensitivity of the tropical Pacific Ocean to precipitation-induced freshwater flux, *Clim. Dyn., 15*, 737–750, 1999.

W. Han, Program in Atmospheric and Oceanic Sciences, University of Colorado, Campus Box 311, Boulder, CO 80309. (whan@monsoon.colorado.edu)

J. P. McCreary, International Pacific Research Center, School of Ocean and Earth Science and Technology, University of Hawaii, 2525 Correa Road, Honolulu, HI 96822. (jay@iprc.soest.hawaii.edu)

K. E. Kohler, Oceanographic Center, Nova Southeastern University, Dania, FL 33004. (kevin@ocean.nova.edu)

(Received May 1, 2000; revised November 8, 2000; accepted November 27, 2000.)